

1 **Projected Changes to Cool-Season Storm Tides in the**  
2 **21st Century along the Northeastern United States**  
3 **Coast**

4 **William J. Pringle<sup>1</sup>, Jiali Wang<sup>1</sup>, Keith J. Roberts<sup>2</sup>, Veerabhadra R.**  
5 **Kotamarthi<sup>1</sup>**

6 <sup>1</sup>Environmental Science Division, Argonne National Laboratory, Lemont, IL, USA

7 <sup>2</sup>School of Marine and Atmospheric Science, Stony Brook University, NY, USA

8 **Key Points:**

- 9 • Cool-season storm tides projected to decrease along the Mid-Atlantic Bight coast  
10 but increase further inland up estuaries and rivers.
- 11 • Arbitrary tide-surge timing strongly affects projected storm tide changes in New  
12 England, New York-New Jersey Bight, and Delaware Bay.
- 13 • Sea level rise is likely to be more critical than storm climatology to future changes  
14 in cool-season coastal flooding potential.

---

Corresponding author: William Pringle, [wpringle@anl.gov](mailto:wpringle@anl.gov)

## Abstract

This study investigates changes and uncertainties to cool-season (November–March) storm tides along the U.S. northeast coast in the 21<sup>st</sup> century under the high RCP8.5 emission scenario compared to late 20<sup>th</sup> century. A high-fidelity (50-m coastal resolution) hydrodynamic storm tide model is forced with three dynamically-downscaled regional climate models (RCMs) over three decadal periods (historical, mid-21<sup>st</sup> century and late-21<sup>st</sup> century) to project future changes in peak storm tide elevations at coastal counties in the region. While there is no absolute consensus on future changes to storm tides, for any one future decade two out of the three RCMs project an increase at counties along the Hudson River, Delaware River and northern Chesapeake Bay due to more intense cyclones that track inland of these locations leading to favorable surge generating conditions. The same RCMs also project a decrease at counties facing the open ocean in the mid-Atlantic Bight as cyclone densities just offshore of the coastline decrease, particularly by late-century. The larger tidal range in northern areas leads to significant uncertainty due to the arbitrary relationship between the local tidal stage and when a surge event occurs, which affects both the magnitude and sign of the projected changes. This tide-surge timing is less important in the Chesapeake Bay and unimportant in Albemarle Sound and Pamlico Sound. Similar to other recent studies, we highlight that sea level rise is likely to be more critical than storm climatology for future changes to the cool-season coastal flooding potential.

## Plain Language Summary

Winter storms (e.g., nor'easters) that develop during the North American cool-season (November to March) can generate high water levels (storm tides) along the northeast coast of the U.S that can potentially result in coastal flooding. This study is concerned with how winter storm tides along the northeastern U.S. coast could change into the 21<sup>st</sup> century under a high emissions climate change scenario. Highly-resolved computer models of the ocean and the atmosphere are used to investigate this question. We find that changes to storm tides are generally less significant than expected sea level rise under the corresponding climate change scenario. However, we find evidence of decreasing storm tides at counties along the Mid-Atlantic Bight coastal region and increasing storm tides at counties along the Hudson River, Delaware River and northern Chesapeake Bay. Expected changes to storm tides are more uncertain in northern areas (New England, Long Island Sound, New York Bight, and Delaware Bay) because of the random timing of the storm and the everyday tide level, which is larger in these areas. Coastal planning should consider the combination of sea level rise and storm tides taking into account the full range of possibilities based on this random tide-storm timing.

## 1 Introduction

Storm surges along the northeastern coast of the United States (herein NEC) are frequently generated by the strong low-level winds and low surface pressures of extra-tropical cyclones (ETCs) that often develop during the North American cool-season months (November to March) (Colle et al., 2013; Booth et al., 2016; Catalano & Broccoli, 2018). Depending on the timing of the surge in relation to the astronomical tide, the resultant storm tide elevation can lead to coastal flooding, in addition to otherwise hazardous marine conditions. Some noteworthy events include the December 27, 2010 nor'easter that induced a ~1-m surge which coincided with high tide causing extensive flooding in Scituate, Massachusetts (Beardsley et al., 2013); and the December 11-12, 1992 nor'easter generated a 1-1.5-m surge around New York City and western Long Island that lasted over three tidal cycles (Colle et al., 2008). The storm tide elevation eventually reached ~2.5-m above mean sea level during high tide at lower Manhattan, resulting in flooding to New York City's subways and train systems (Colle et al., 2010).

65 While often less severe than hurricane-driven surge, ETCs are responsible for most  
66 moderate surge events in the NEC region and affect a very wide region of the coastline  
67 (Booth et al., 2016). It is thus important to assess the impacts of ETC-driven surge and  
68 storm tides, especially when considering events of moderate frequency (1- to 3-year timescales).  
69 Systematic changes to ETCs under a changing climate could affect the frequency and  
70 severity of cool-season storm tides leading to more (or less) frequent coastal flooding. For  
71 instance, it has been shown that large ETC-driven surges along the NEC are typically  
72 generated by slow-moving deep cyclones to the south of a strong anticyclone (Catalano  
73 & Broccoli, 2018), so changes in these types of events would play a critical role in al-  
74 tering the frequency of ETC-driven coastal flooding events. Furthermore, any changes  
75 to storm tides must be viewed with respect to rising sea levels that would further en-  
76 hance the risk to coastal flooding (Booth et al., 2016), so it is also important to put the  
77 magnitudes of each into context.

78 Several studies have explored the effects of global warming on cool-season ETC cli-  
79 matology for the NEC. Most of these project a reduction in the density of ETCs over  
80 the continental United States and western North Atlantic Ocean (Teng et al., 2008; Long  
81 et al., 2009; Chang, 2013; Colle et al., 2013; Seiler et al., 2018). ETC intensities over the  
82 western North Atlantic Ocean are also predicted to weaken, however cyclones may be-  
83 come more intense and deepen more rapidly just inland of the NEC (Colle et al., 2013).  
84 Many of these studies used output from global climate models (GCMs), particularly those  
85 from phase 5 of the Coupled Model Intercomparison Project (CMIP5; Taylor et al., 2012)  
86 which have horizontal model resolutions of  $\sim 100$ - $300$  km. Due to the regional differences  
87 and dependence on model resolution, Colle et al. (2013) suggests that dynamically down-  
88 scaled regional versions of the GCMs are needed to investigate the changes to ETC track  
89 density and intensification in more detail. Other studies show that 20-km horizontal res-  
90 olution dynamically downscaled regional climate models (RCMs) generate stronger cy-  
91 clones than the parent GCMs based on the surface wind speed (Booth et al., 2018; Zhang  
92 & Colle, 2018). The downscaled simulations also indicated that latent heating related  
93 diabatic processes, which are otherwise too weak in coarse-resolution GCMs, could en-  
94 hance development of intense ETCs over the NEC (Zhang & Colle, 2018). However, stud-  
95 ies by Long et al. (2009); Seiler et al. (2018) suggest that projected changes to ETC den-  
96 sity are not particularly sensitive to model resolution.

97 Previous studies have examined climate change impacts on cool-season surge along  
98 the NEC using statistical (Roberts et al., 2017) or hydrodynamic (Lin et al., 2019) surge  
99 models forced by surface winds and pressure from CMIP5 GCM ensembles. Roberts et  
100 al. (2017) found no significant change to surge return intervals in a future period (2054-  
101 79) compared to a historical period (1974-2004) at The Battery in New York City. This  
102 was attributed to the fact that projected ETC changes did not occur in regions that favor  
103 the generation of surge at The Battery. Similarly, Lin et al. (2019) found relatively  
104 small projected changes ( $<7\%$ ) to extreme storm surge heights for the same future pe-  
105 riod along most of the NEC, while noting however that one of the GCMs showed a more  
106 substantial increase of up to 36% for the 50-year surge height. These previous analyses  
107 contain uncertainties due to the usage of atmospheric forcings from coarsely resolved GCMs  
108 and surge prediction by straightforward multilinear regression (Roberts et al., 2017) or  
109 a relatively coarse resolution hydrodynamic model ( $\sim 1$ -km coastal resolution; Lin et al.,  
110 2019). Furthermore, astronomical tides were omitted even though it is the combination  
111 of surge and tide (storm tide) that needs to be considered to assess local flooding po-  
112 tential (Horsburgh & Wilson, 2007). In this study, we address these limitations by in-  
113 tegrating results from three 12-km dynamically downscaled RCMs with a high-fidelity  
114 ( $\sim 50$ -m coastal resolution) hydrodynamic storm tide model, which we run multiple times  
115 to account for the arbitrary surge-tide phasing. Using this high-resolution integrated mod-  
116 eling system we aim to: 1) quantify projected changes and associated uncertainties of  
117 cool-season storm tides in the 21<sup>st</sup> century along the NEC as compared to estimates of

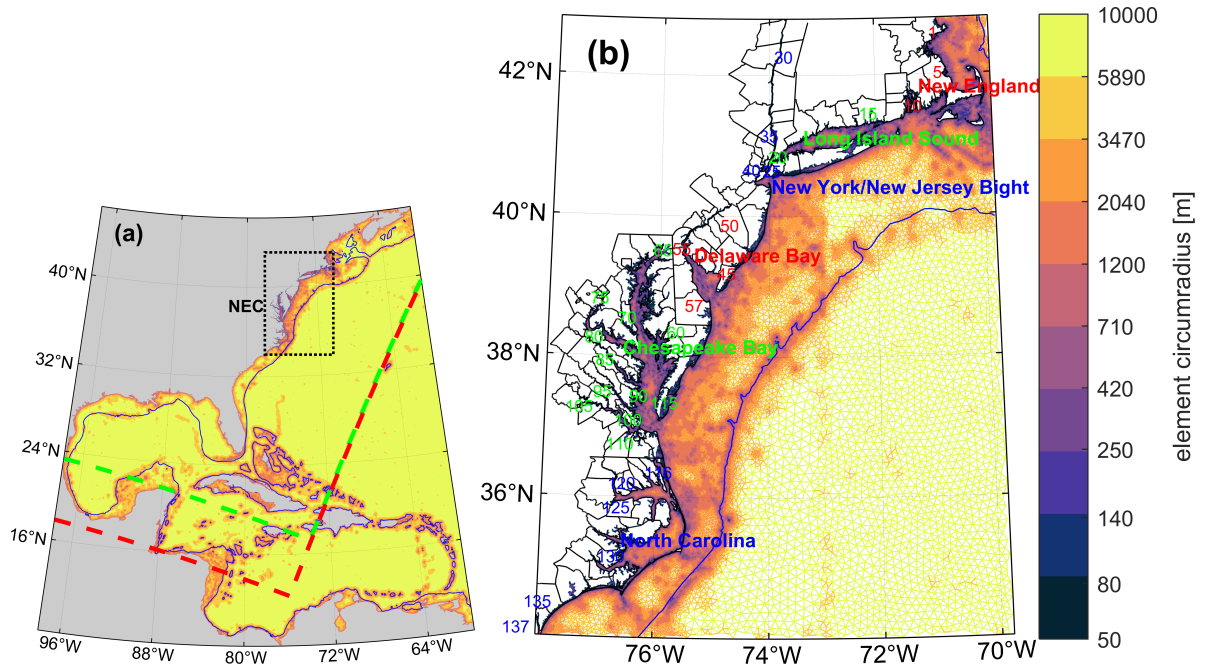


**Figure 1.** Computational domain and unstructured mesh resolution of the ADCIRC hydrodynamic storm tide model. (a) Full extent of the computational domain covering the western North Atlantic Ocean. The blue line demarcates the 200-m depth contour – approximate edge of the continental shelf. Dashed outlines indicate the boundary of the WRF-based regional climate models used to force the storm tide model (WRF-CCSM4: green, WRF-GFDL/HadGEM2: red). The dashed black box indicates the NEC region that is shown in more detail in panel (b). Coastal counties (partially numbered in this figure; see spreadsheet datasets in Pringle (2020) for full county numbering and metadata) are demarcated by the black outlines. The colored labels (corresponding to proximate counties of the same color) indicate locations of the different sub-regions focused on in this study.

118 sea level rise (SLR), and 2) relate projected storm tide changes to the ETC climatology,  
 119 such as changes to track patterns and intensity.

120 The rest of this paper is organized as follows: first we introduce the modeling and  
 121 analysis approach in Sect. 2; in Sect. 3 we present results showing model accuracy dur-  
 122 ing the historical period, followed by our projected changes to storm tides in future decades  
 123 and the associated ETC patterns driving these storm tide changes; in Sect. 4 we discuss  
 124 our major findings and their implications, as well as the uncertainties and limitations  
 125 of the study.

## 126 2 Methods

### 127 2.1 Dynamically Downscaled Regional Climate Model Experiments

128 Three sets of CMIP5 GCMs (CCSM4, GFDL-ESM2G and HadGEM2-ES) have been  
 129 dynamically downscaled to 12 km horizontal resolution using the Weather Research and  
 130 Forecasting (WRF) v3.3.1 model (Wang & Kotamarthi, 2015; Zobel et al., 2018). These  
 131 three GCMs were chosen based on evidence that they approximately represent the spread  
 132 of climate sensitivity for the 30 GCMs in the CMIP5 experiment (GFDL-ESM2G – lower  
 133 sensitivity, CCSM4 – moderate sensitivity, HadGEM2-ES – high sensitivity) (Sherwood

134 et al., 2014; Zobel et al., 2018). Herein, the downscaled RCMs are referred to as WRF-  
 135 CCSM4, WRF-GFDL and WRF-HadGEM. The WRF computational domains cover all  
 136 of the continental USA (see Fig. S1) extending out to the western North Atlantic Ocean  
 137 to encompass all of the U.S. East Coast and Gulf Coast, and parts of the Caribbean (Fig. 1).  
 138 Sea level pressures (SLP) and 10-m wind velocities (U10; both zonal and meridional di-  
 139 rections) are output from the model simulations at 3-hourly intervals and used to forced  
 140 the hydrodynamic storm tide model.

141 Each RCM provides meteorological data for three decadal periods; 1995-2004 (“his-  
 142 torical” decade), 2045-2054 (“mid-century” decade), and 2085-2094 (“late-century” decade).  
 143 This corresponds to nine continuous cool-seasons for each decade, e.g., November 1995-  
 144 March 1996 to November 2003-March 2004 for the historical decade. The future decades  
 145 were simulated under the Representative Concentration Pathway (RCP) 8.5, a pathway  
 146 that assumes high levels of greenhouse gas emissions by 2100 with an effective radiative  
 147 forcing increase of  $8.5 \text{ W/m}^2$  due to a large global population and little technological im-  
 148 provement (Riahi et al., 2011). Recent estimates predict that RCP8.5 will accurately rep-  
 149 resent current emissions out until mid-century and represents at least plausible levels out  
 150 until late-century (Schwalm et al., 2020).

## 151 2.2 Hydrodynamic Storm Tide Model

152 The ADvanced CIRCulation (ADCIRC) hydrodynamic model (Luettich & Wes-  
 153 terink, 2004) is used to simulate storm tides along the NEC. We use Version 55 of the  
 154 model that newly incorporates self-attraction and loading (SAL) tides, internal tide in-  
 155 duced wave drag, and modifications to the governing equations to correctly account for  
 156 Earth’s curvature (Pringle et al., 2020). The ADCIRC computational domain covers the  
 157 western North Atlantic Ocean west of the  $60^\circ$  meridian (Fig. 1a), a well-studied region  
 158 for the ADCIRC model (e.g., Westerink et al., 2008; Bunya et al., 2010; Hope et al., 2013;  
 159 Marsooli & Lin, 2018; Roberts, Pringle, Westerink, Contreras, & Wirasaet, 2019). Ver-  
 160 sion 3 (Pringle & Roberts, 2020) of OceanMesh2D (Roberts, Pringle, & Westerink, 2019)  
 161 is used to automatically generate an unstructured mesh for the study domain using care-  
 162 fully designed combinations of shoreline geometry and seabed topography-based element  
 163 sizing functions (cf. Roberts, Pringle, Westerink, Contreras, & Wirasaet, 2019). A nom-  
 164 inal minimum element size concentrated at the coast is set to 50 m in the NEC region  
 165 and 1 km elsewhere (Fig. 1). The nominal maximum element size in the deep ocean is  
 166 set to 10 km. Mesh bathymetry is interpolated from the high-resolution ( $\sim 1\text{-}3\text{-m}$ ) USGS  
 167 Coastal National Elevation Database (CoNED) in the NEC region and  $\sim 500\text{-m}$  SRTM15+  
 168 (Tozer et al., 2019) Version 2 data elsewhere.

169 The storm tide model is forced with SLP and U10 (both zonal and meridional di-  
 170 rections) from the downscaled WRF climate model data, in addition to astronomical tidal  
 171 potential and SAL for the eight dominant tidal constituents ( $M_2$ ,  $S_2$ ,  $N_2$ ,  $K_2$ ,  $K_1$ ,  $O_1$ ,  
 172  $P_1$ ,  $Q_1$ ). Astronomical tides are also prescribed at the open boundary using the TPXO9-  
 173 Atlas (Egbert & Erofeeva, 2019). To account for the random timing between tides and  
 174 storm-driven surge we simulate each season five times with different tidal phases (-10,  
 175 -5, +0, +5, +10 hour offsets from the actual date-time). A computational time step of  
 176 12 s was used for all simulations, and water elevations were output at 1 hour intervals  
 177 for the analysis.

## 178 2.3 Peak Storm Tide Elevations

179 For each decade and each realization of the five tidal phases we extracted Peak Storm  
 180 Tide elevations (PST) separated by a minimum of 3 days from the data to identify unique  
 181 ETC-driven events (Lin et al., 2019). In previous studies this data has been processed  
 182 into extreme value estimates of low frequency PST events, e.g., 50-year and 100-year re-  
 183 turn periods, obtained by fitting the tail of extracted peaks to the Generalized Pareto

184 Distribution using the Peak Over Threshold method (Lin et al., 2019; Marsooli et al.,  
 185 2019). However, we deemed the decadal-long simulations in this study to be too short  
 186 to conduct a robust extreme value analysis. We instead choose to measure changes in  
 187 PST for return periods contained within the time period of the simulations; the 3-season  
 188 and 1-season return periods. We define the 3-season PST empirically as the third high-  
 189 est PST within a decade (i.e., the third largest in nine cool seasons); while the 1-season  
 190 PST is defined as the ninth highest PST within a decade.

191 Simulated PST values are reduced to a single value for each county along the NEC  
 192 coast (Fig. 1) so that the results are more easily presented and understood (these results  
 193 are described in Sects. 3.2-3.3). The value for each county is taken as the maximum PST  
 194 at the mesh vertices along the coastline of that county (c.f. Marsooli et al., 2019). For  
 195 comparison, the astronomical MHHW (mean higher high water) value for each county  
 196 is also approximated from harmonic constituent amplitudes ( $\approx 1.1M_2 + K_1 + O_1$  – half  
 197 of the sum of the mean range and diurnal range, Parker, 2007). Differences in the county-  
 198 wide PST values between future and historical decades are presented individually for each  
 199 RCM forcing. The tidal phase related uncertainty in the difference is found by taking  
 200 the minimum, mean and maximum differences of all possible combinations of tidal phase  
 201 in the future and historical decade (25 total).

202 Furthermore, we compare the relative magnitude of storm tide changes to SLR under  
 203 the RCP8.5 scenario, which is computed for each county from the ocean model out-  
 204 puts of the three parent GCMs. SLR is approximated as the difference between the fu-  
 205 ture cool-season decadal average and the historical cool-season decadal average of the  
 206 total sea surface height in the closest GCM ocean point to the county midpoint. We de-  
 207 fine the total sea surface height as the sea surface height (CMIP5 variable *zos*) plus the  
 208 global average steric sea level change (CMIP5 variable *zossga*) (Becker et al., 2016)

## 209 **2.4 Cyclone Tracking and Mapping to Peak Storm Tides**

210 To attribute changes in storm tides to patterns of ETC tracks and intensities, we  
 211 extracted storms from the meteorological data by tracking the local minimums of SLP  
 212 using Version 2 of CycloneTrack (Flaounas et al., 2014), a cyclone tracking algorithm.  
 213 To filter out small scales in SLP a 2-D Gaussian smoothing kernel with a standard de-  
 214 viation of 10 is used.

215 We select ETC tracks that produce a large peak storm tide elevation within one  
 216 of the following six multi-county subregions: New England (NE), Long Island Sound (LIS),  
 217 New York/New Jersey Bight (NY/NJ), Delaware Bay (DB), Chesapeake Bay (CB), and  
 218 North Carolina (NC) (Fig. 1). Tracks are selected by finding those that exist within the  
 219 NEC domain just before and after the time of the peak storm tide. Usually there is just  
 220 one track that meets this criteria, but sometimes there are no tracks in which we skip  
 221 to the next highest peak storm tide elevation, or very occasionally there are two tracks  
 222 in which we record both. Using this methodology, in Sect. 3.4 we present the ETC tracks  
 223 from the nine highest PST for each RCM for each subregion.

## 224 **3 Results**

### 225 **3.1 Historical Decade Model Accuracy**

#### 226 **3.1.1 Dynamically Downscaled Regional Climate Model**

227 Figures showing the historical accuracy of the WRF-based RCM simulations com-  
 228 pared to offshore buoy observations and ERA5 reanalysis data (European Centre for Medium-  
 229 Range Weather Forecasts, 2019) are presented in the supplementary material. Low-level  
 230 winds in the RCMs during the historical decade are shown to be mostly accurate (RMSE  
 231  $< 0.6$  m/s) at offshore buoy locations and in the northern part of the NEC region, while

errors are largest (RMSE up to 2.4 m/s) near the North Carolina and Virginia coast-  
line (Fig. S2). Higher errors at the coast could be due to land-masking and geopotential  
height discrepancies in the WRF model. There is a tendency for southeasterly-southwesterly  
winds speeds to be overestimated and westerly-northwesterly wind speeds to be slightly  
underestimated throughout the region (Fig. S3-S5).

Compared to ERA5, the density distribution of simulated ETCs in the NEC region  
are shown to be accurate to within 1-2 cyclones/season for all the RCMs (Fig. S6),  
showing improvements over the parent GCMs which tend to underestimate cyclone densities  
further (Roberts, 2015). WRF-CCSM4 underestimates the density of ETCs offshore  
while WRF-HadGEM overestimates. WRF-GFDL overestimates cyclone density closer  
to the coast especially near the New Jersey and New York region. Compared to ERA5,  
WRF-CCSM4 shows good agreement in the shape of the distribution of ETC maximum  
lifecycle intensities [minimum SLP (Pmin) and maximum U10 (Umax)], but it produces  
too few of the most frequently observed cyclones (Pmin  $\sim$ 990-1010 hPa, Umax  $\sim$ 14-  
24 m/s; Fig. S7). The WRF-GFDL and WRF-HadGEM produce a greater overall number  
of ETCs than WRF-CCSM4, which matches more closely with ERA5 (Fig. S7). However,  
there are more ETCs of greater intensity (Pmin  $<$  990, Umax  $>$  24 m/s) than in ERA5.  
Similarly, Figs. S3-S5 show that the 95% quantile wind speeds against offshore buoys  
are more overestimated in WRF-GFDL and WRF-HadGEM RCMs than in WRF-CCSM4.

### 3.1.2 Hydrodynamic Storm Tide Model

The historical accuracy of the hydrodynamic storm tide model simulations have  
been assessed based on computing root-mean-square errors (RMSE) from quantile-quantile  
plots of daily maximum water levels (DMWL). Errors are within 0.2 m throughout most  
of the NEC (Fig. 2); the tidal range at one tide gauge in a complex wetland environment  
(Wachapreague, VA) is overestimated by the model leading to the highest errors there  
(RMSE  $\sim$  0.3 m). The errors of the RCM-forced runs are distributed similarly to those  
under the ERA5 reanalysis forcing, partly because both surge and tidal components contribute  
to the DMWL. The greatest difference in DMWL errors between the atmospheric forcings  
is found in Delaware Bay and Chesapeake Bay. Wind speed errors (Fig. S2) just offshore  
of Delaware Bay and Chesapeake Bay were shown to be largest for the WRF-HadGEM  
model which could be contributing to the also generally larger associated DMWL errors  
in these estuaries. Wind speed errors inside Chesapeake Bay is greatest for WRF-CCSM4  
and associated DMWL errors throughout Chesapeake Bay are indeed larger than those  
under ERA5 and WRF-GFDL forcing.

The simulated 3-season PST (mean of the five tidal phase realizations) during the  
historical decade at each mesh vertex in the NEC region under ERA5 reanalysis and RCM  
forcing is shown in Fig. 3. Furthermore, the 3-season and 1-season PST are compared  
to selected NOAA tide gauges in the NEC region in Fig. 4 using error bars to indicate  
the tidal phase-based uncertainty, whereas the observational data (demeaned for each  
season) is a single realization of the tidal phase. This uncertainty is greater for the lower  
frequency 3-season PST (Fig. 4a) than the 1-season one (Fig. 4b), and is greatest along  
the stretch of coastline from Woods Hole to Atlantic City tide gauges under WRF-GFDL  
forcing. Although the spatial distribution of PSTs are similar under all meteorological  
forcing since it is heavily related to the tidal range, the RCM forcing consistently generates  
greater storm tide elevations than the reanalysis forcing. The RCM-forced PSTs are  
indeed overestimated at some tide gauges, in particular those in the Long Island Sound  
and Delaware Bay (Woods Hole to Montauk, Philadelphia and Reedy Point). However,  
it is equally true that PSTs under reanalysis forcing are underestimated at many of the  
tide gauges, which could mean that the most extreme winds are smoothed-out in the  
reanalysis data compared to the RCMs.

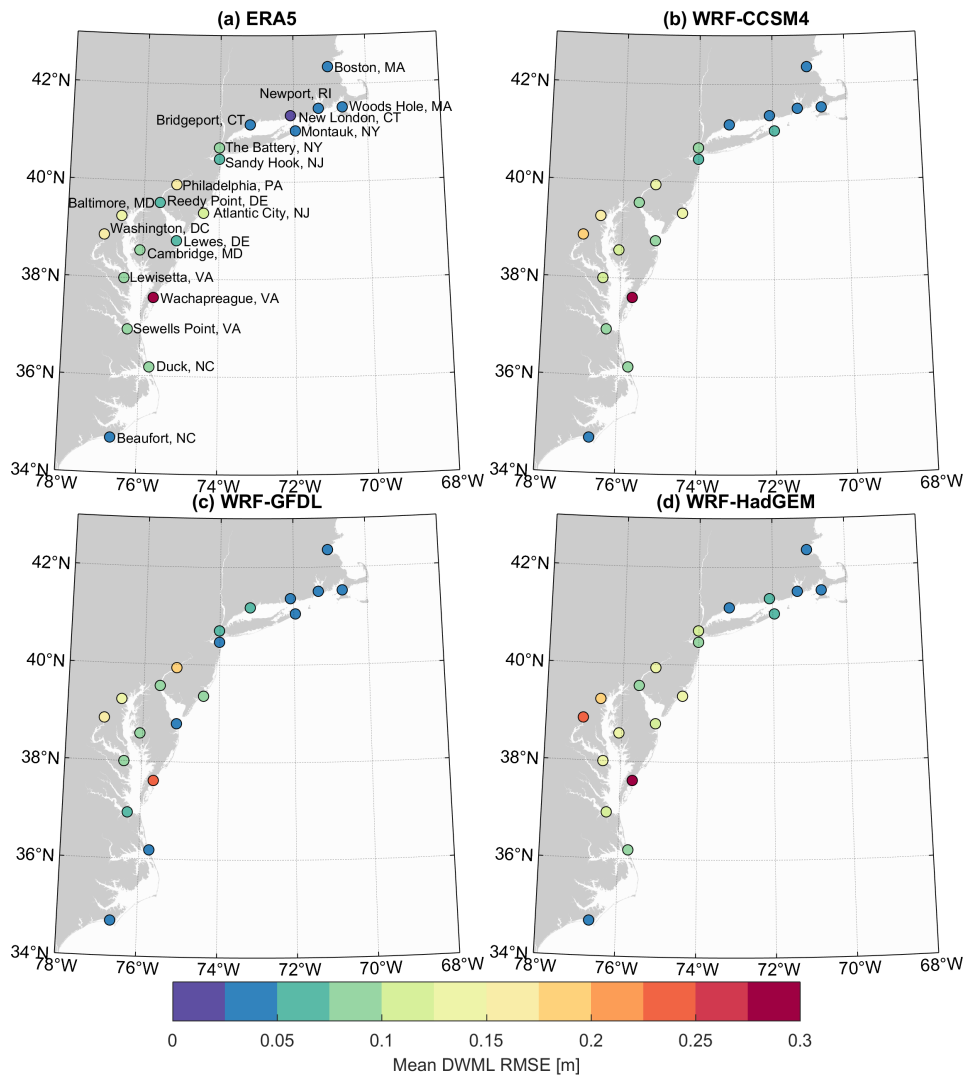


**Figure 2.** Accuracy (mean RMSE from the five tidal-phase realizations) of daily maximum water levels (DMWL) simulated by the hydrodynamic model at NOAA tide gauges in the NEC region for the historical cool-season decade (1995-2004). The hydrodynamic model was driven by atmospheric forcing from (a) ERA5 reanalysis, (b) WRF-CCSM4, (c) WRF-GFDL, (d) WRF-HadGEM.

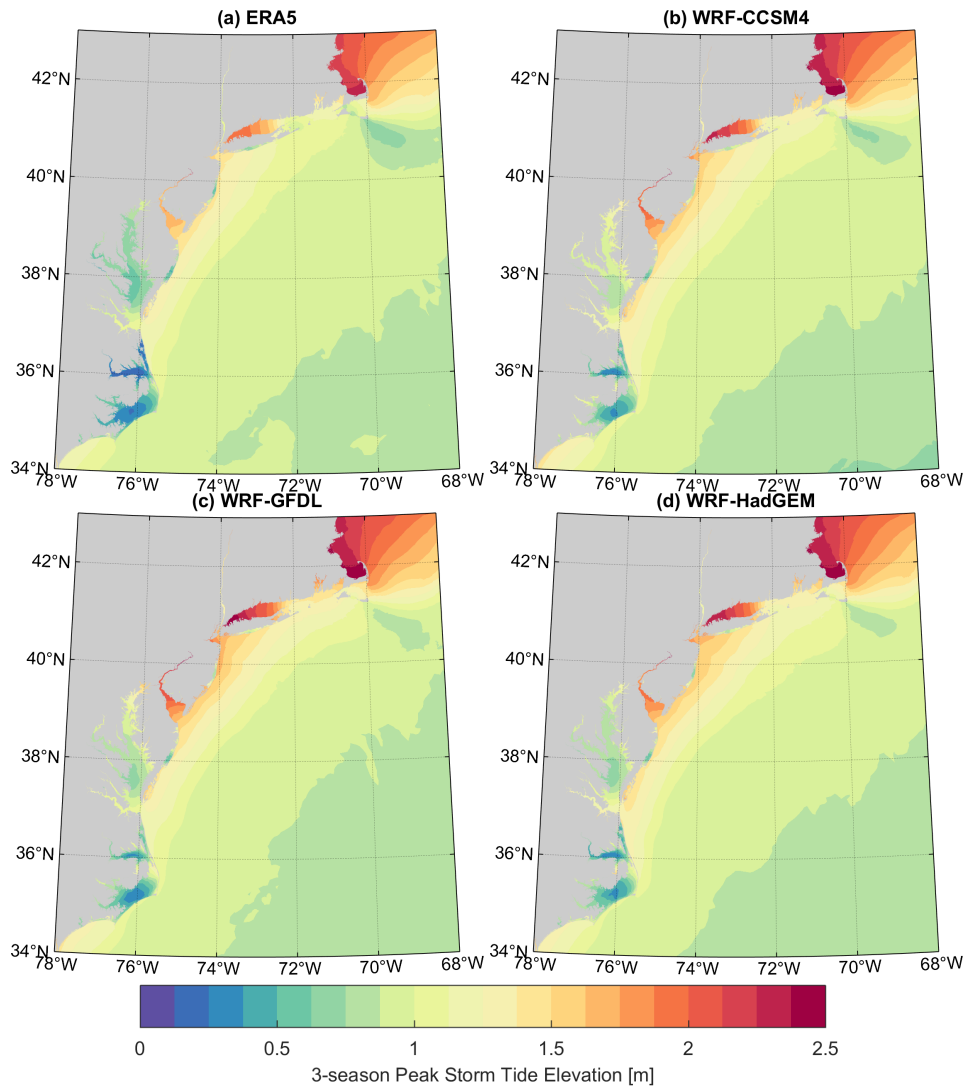


**Figure 3.** Comparison of the hydrodynamic model simulated 3-season PST (peak storm tide elevation) in the NEC region for the historical cool-season decade (1995-2004). Results shown are the mean of the five tidal phase realizations simulations for each meteorological forcing: (a) ERA5 reanalysis, (b) WRF-CCSM4, (c) WRF-GFDL, (d) WRF-HadGEM.

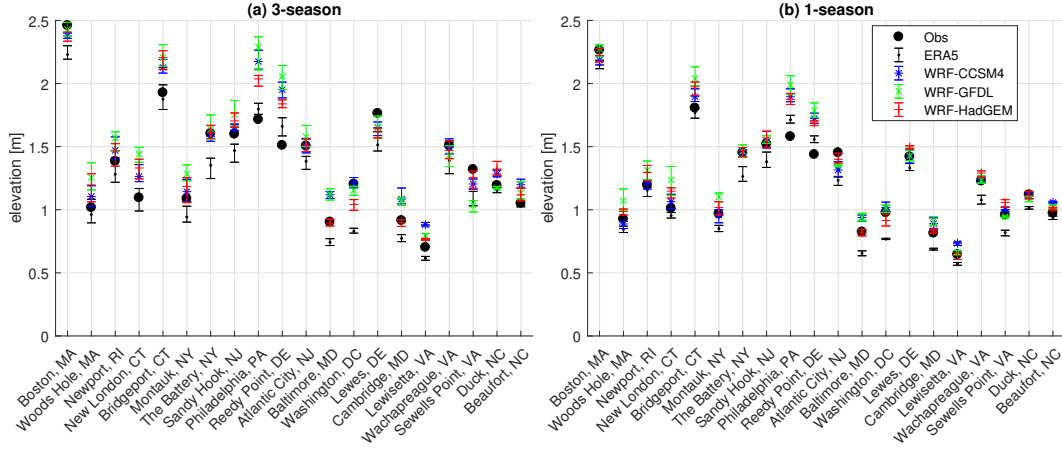


**Figure 4.** Comparison of observed and simulated (a) 3-season and (b) 1-season PST (peak storm tide elevations) at NOAA tide gauges in the NEC region (locations shown in Fig. 2) for the historical cool-season decade (1995-2004) under various meteorological forcing. The error bars indicate the mean and upper/lower bounds for the five tidal phase realizations.

283

### 3.2 Peak Storm Tide Elevation Changes in Mid-Century Decade

284

Projected PST changes range within  $\pm 0.4$  m for the 3-season PST (Fig. 5b) and  $\pm 0.3$  m for the 1-season PST (Fig. 6b) throughout the NEC region for the three RCM forcings by mid-century. The magnitude of the 3-season PST changes by mid-century across the NEC are of similar order to SLR under the CCSM4 and GFDL SLR scenarios ( $\sim 0.2$  m). However, the magnitude of SLR according to HadGEM (0.6-0.8 m) is significantly larger than 3-season PST changes. The magnitude of 1-season PST changes by mid-century across the NEC are slightly smaller in magnitude to CCSM4/GFDL SLR ( $\sim 0.2$  m), and much smaller than HadGEM SLR (0.6-0.8 m).

292

In the northern counties ( $< \#60$ ) projected PST changes are highly dependent on the RCM forcing. WRF-CCSM4 forcing results in mostly small average (tidal phase-based) increases to PSTs in the New England, Long Island Sound, and New York/New Jersey Bight subregions and up to as large as 0.15 m along the Delaware River (#47-55) in the Delaware Bay subregion. Similarly, WRF-HadGEM forcing projects on average mostly small increases to the 3-season PST, where larger increases up to 0.2 m are recorded throughout most of the New York/New Jersey Bight subregion, at Rhode Island counties (#10-14) in the New England subregion, and at counties along the Delaware River. For the 1-season PST, WRF-HadGEM projects mostly little change but localized increases ( $\sim 0.1$  m) for counties along the Hudson River (#30-34), and decreases (0.05-0.15 m) for counties #40-45 and #56-58, which are located along the New Jersey coastline and at the entrance to Delaware Bay, facing the open ocean. In contrast, the WRF-GFDL run shows an average decrease to PSTs at all of the northern counties at magnitudes of 0.1-0.3 m for the 3-season and  $\sim 0.1$  m for the 1-season. The tidal phase-based variability of these changes in these northern counties is comparatively large at 0.3-0.5 m for the 3-season PST and 0.15-0.3 m for the 1-season PST under all RCMs, which is larger than most of the tidal phase-based average changes.

309

For southern counties ( $> \#60$ ), WRF-CCSM4 and WRF-HadGEM forcings largely project average decreases. While little change to PSTs is seen in the central west regions of Chesapeake Bay (counties #60-90), fairly large average decreases are projected under these two RCM forcings elsewhere, up to 0.2 m-0.3. Comparatively, the WRF-GFDL run projects mostly small average increases to PSTs of  $\sim 0.2$  m for 3-season and  $\sim 0.1$

313

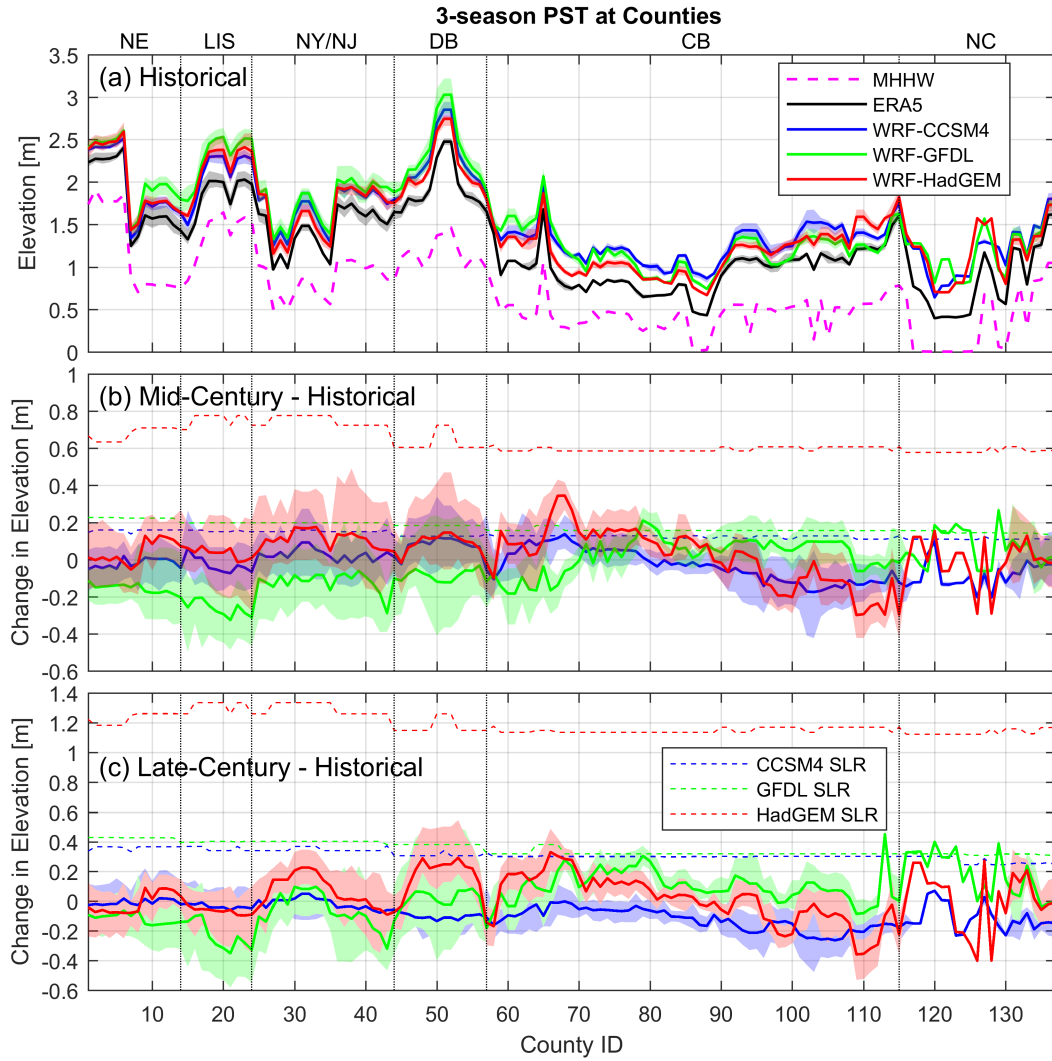


**Figure 5.** Simulated 3-season PST (peak storm tide elevations) at counties along the NEC coastline (see Fig. 1 for locations) during the cool-season under various meteorological forcing). (a) Historical decade (1995-2004) including the modeled astronomical MHHW, (b) Mid-century decade (2045-2054) minus historical decade, (c) Late-century decade (2085-2094) minus historical decade. Solid lines show the tidal phase-based mean and the translucent bands show the tidal phase-based range. The dashed lines in (b) and (c) indicate the decadal mean increase in sea level (SLR) compared to the historical decade for the parent GCMs. NE: New England, LIS: Long Island Sound, NY/NJ: New York/New Jersey Bight, DB: Delaware Bay, CB: Chesapeake Bay, NC: North Carolina.

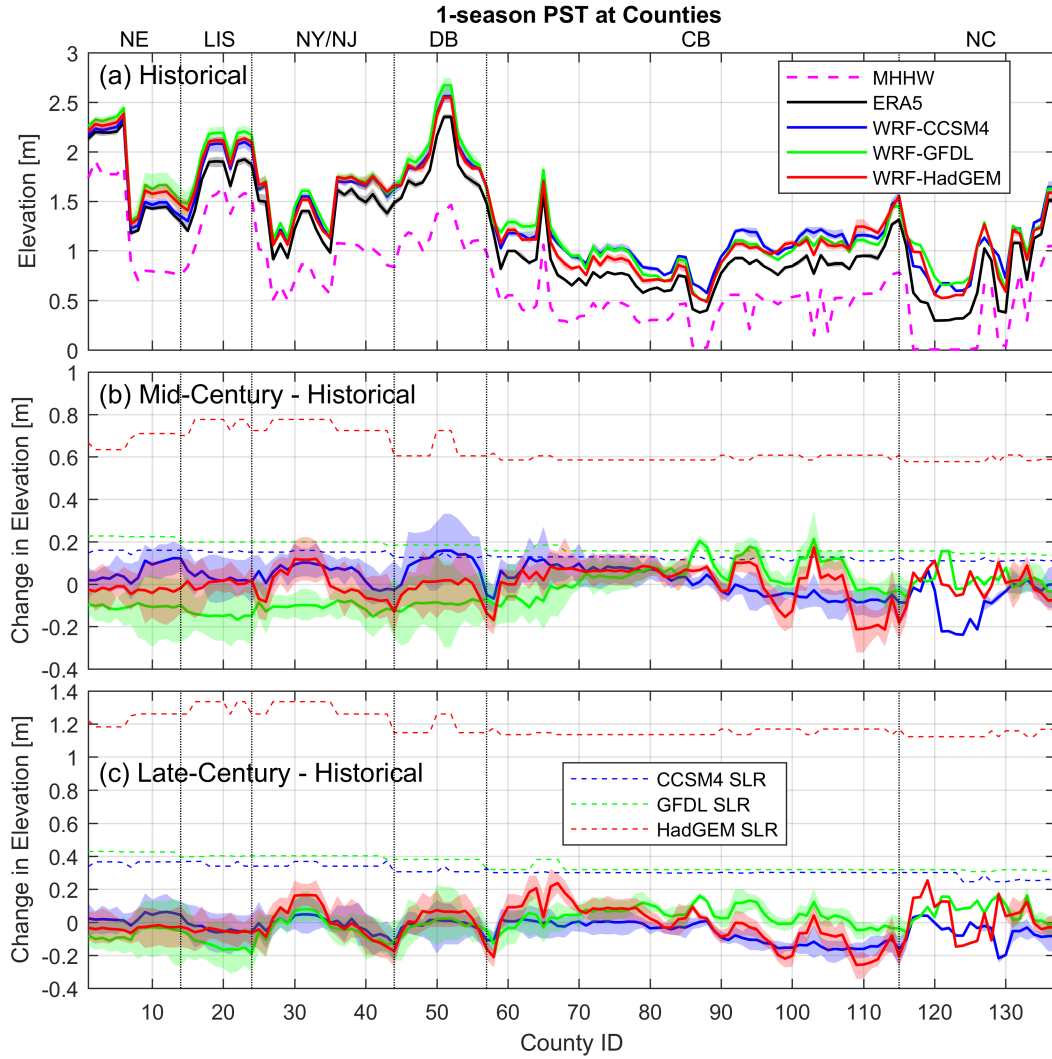


**Figure 6.** Same as Fig. 5 but for 1-season PST.

314 m for the 1-season in these southern counties. Localized larger average increases of  $\sim 0.15$ -  
 315  $0.2$  m to the 1-season PST are noticeable at counties located up western tributaries of  
 316 Chesapeake Bay and Albemarle Sound (#86-88, #94-95, #103, #121-122). The tidal  
 317 phase-based variability is not very significant for these southern counties, especially for  
 318 those in the north part of the North Carolina subregion. This area corresponds to Albe-  
 319 marle and Pamlico Sounds that have a tidal range of only a few centimeters (refer MHHW  
 320 in Fig. 5a), and hence susceptible to changes in PST due to locally generated storm surge  
 321 only.

### 322 **3.3 Peak Storm Tide Elevation Changes in Late-Century Decade**

323 Projected PST changes range within  $\pm 0.5$  m for the 3-season PST (Fig. 5c) and  
 324  $\pm 0.3$  m for the 1-season PST (Fig. 6c) throughout the NEC region for the three RCM  
 325 forcings by late-century. In this decade the WRF-GFDL and WRF-HadGEM forcings  
 326 project changes that have a high-degree of spatial variability, while WRF-CCSM4 shows  
 327 smaller and smoother changes. The magnitude of the 3-season PST changes in late-century  
 328 across the NEC are similar to but mostly smaller in magnitude to SLR under the CCSM4

and GFDL SLR scenarios ( $\sim 0.4$  m). The magnitude of SLR according to HadGEM (1.1-1.3 m) is far greater than the 3-season PST changes; it is at least two times the size of the greatest PST decrease for any run and county. The magnitude of the 1-season PST changes by late-century across the NEC are all smaller (at least slightly) in magnitude to CCSM4/GFDL SLR ( $\sim 0.4$  m), and are completely dwarfed by HadGEM SLR (1.1-1.3 m).

In the northern counties ( $< \#60$ ), WRF-CCSM4 forcing projects only very small average (tidal phase-based) changes to the 3-season PST in the New England, Long Island Sound, and New York/New Jersey Bight subregions and a decrease of  $\sim 0.1$  m in the Delaware Bay subregion. Also under WRF-CCSM4 forcing, the 1-season PST is mostly unchanged in these northern counties except for a decrease of  $\sim 0.1$  m for counties near the entrance to Delaware Bay ( $\#44$  and  $\#58$ ) facing the open ocean. In most of the northern counties, WRF-HadGEM forcing projects very small average changes to the 3-season PST, however there are large increases ( $\sim 0.2$ - $0.3$  m) along the Hudson River ( $\#30$ - $33$ ) and Delaware River ( $\#47$ - $55$ ). For the 1-season PST, WRF-HadGEM projects average increases of  $0.15$ - $0.25$  m at counties along the Hudson River and average decreases of  $\sim 0.2$  m for counties near the entrance to Delaware Bay ( $\#44$  and  $\#58$ ) facing the open ocean (also true for WRF-GFDL). Comparatively, WRF-GFDL forcing projects mostly average decreases to PSTs for northern counties (up to  $0.35$  m for the 3-season and  $0.2$  m for the 1-season). However, there are increases, although smaller ( $< 0.1$  m) than for WRF-HadGEM, at the same Hudson River and Delaware River counties.

For the southern counties ( $> \#60$ ), WRF-GFDL projects mostly increases to PSTs – up to  $0.5$  m for the 3-season but only up to  $0.15$  m for the 1-season – and WRF-CCSM4 projects mostly decreases – up to  $0.25$  m for the 3-season and  $0.15$  m for the 1-season. WRF-HadGEM forcing shows more spatial variability to projected PST changes. For instance, WRF-HadGEM projects average increases to the 1- and 3-season PSTs of  $0.15$ - $0.3$  m at northern Chesapeake Bay ( $\#63$ - $69$ ), and northern Albemarle Sound ( $\#117$ - $119$ ) counties, but average decreases of up to  $0.25$ - $0.3$  m at counties in the southwest portion and at the entrance of Chesapeake Bay ( $\#96$ - $115$ ). There is no RCM-wide consensus in the North Carolina subregion with average changes ranging from 3-season PST decreases up to  $0.4$  m for WRF-HadGEM to increases of  $0.4$  m for WRF-GFDL. The same is true for 1-season PST changes but the variation between RCM forcings is smaller in magnitude ( $\pm 0.2$  m).

### 3.4 Cool-season Storm Climatology Patterns Driving Storm Tide Changes

In the northern subregions (New England, Long Island Sound, New York/New Jersey Bight) during the historical period, many of the RCM-simulated highest nine peak storm tide generating ETC tracks tend to follow nearby and parallel to the coastline (Figs. 7). In the future decades ETC tracks tend to be more sparsely distributed and are less likely to follow that coastline parallel track, either veering further offshore or tracking more inland in the south-to-north direction. Specifically, in WRF-GFDL there are fewer storms that make close or direct impact to the subregion of concern which could explain why WRF-GFDL forced PSTs are projected to mostly decrease in the northern subregions in future decades. However, WRF-GFDL forced PSTs are projected to increase in the Hudson River in the late-century decade. It is noticeable that all WRF-GFDL decades produce storms that pass through the northern New York/New Jersey Bight subregion where Hudson River is located, but in the late-century the storm tracks are clustered further to the north than the other two decades. Due to the anticlockwise cyclone rotation, southerly winds which would be favorable to surge generation in the river are to the southeast of the cyclone center. Similarly, WRF-HadGEM shows a number of relatively intense storms tracking just inland of the Long Island Sound and New York/New Jersey Bight subregions in the south-to-north direction in future decades, particularly in the mid-century. Future PSTs under WRF-HadGEM forcing are largely increased in the Hud-

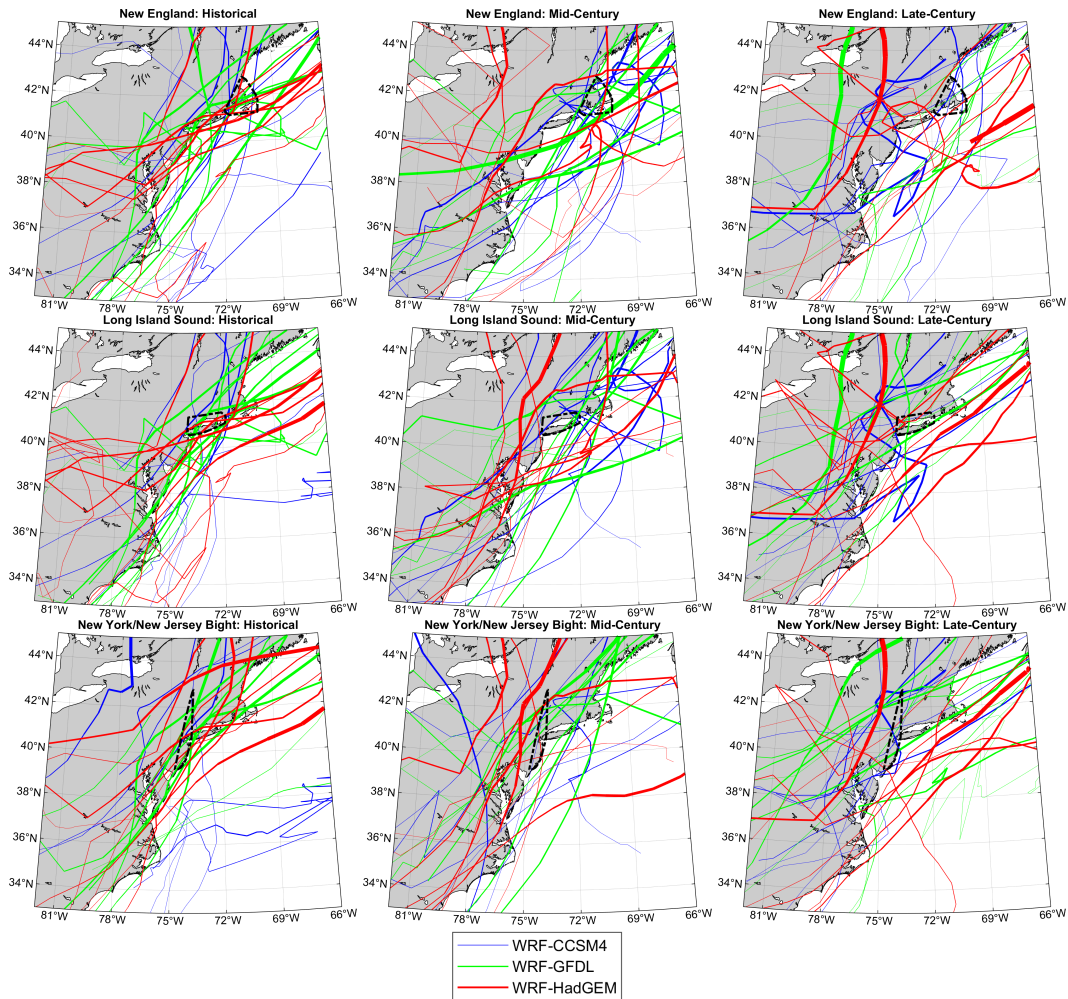


**Figure 7.** Distribution of regional climate model (RCM)-simulated cool-season ETC tracks that produce the nine highest peak storm tide elevations under each RCM forcing within a northern subregion as indicated by the black dashed-line polygon (top: New England, middle: Long Island Sound, bottom: New York/New Jersey Bight). The tracks are color coded according to the RCM and line thicknesses are proportional to ETC intensity ( $P_{min}$ , lower is thicker). Tracks are shown for the three decades investigated in this study (left-to-right): Historical (1995-2004), Mid-century (2045-2054), and Late-century (2085-2094).

381 son River as well as in west New England and east Long Island Sound counties for the  
 382 3-season PST. In the historical period most WRF-HadGEM storms generating surge in  
 383 the New England and Long Island Sound subregions passing to just offshore at southwest-  
 384 to-northeast direction which are likely not as favorable to generating surge as storms that  
 385 track further inland in the south-to-north direction. The WRF-CCSM4 RCM meanwhile  
 386 shows more storms passing through or close to the subregions in the future decades than  
 387 the historical one, and the storms are somewhat more intense. WRF-CCSM4 forcing showed  
 388 increases to the 1-season PST in both future decades (greater increase in the mid-century)  
 389 at the west New England and Hudson River counties. However, the WRF-CCSM4 storms  
 390 are not as intense as some of those in future WRF-GFDL/WRF-HadGEM simulations,  
 391 potentially explaining why the lower frequency 3-season PST under WRF-CCSM4 forc-  
 392 ing is largely unchanged.

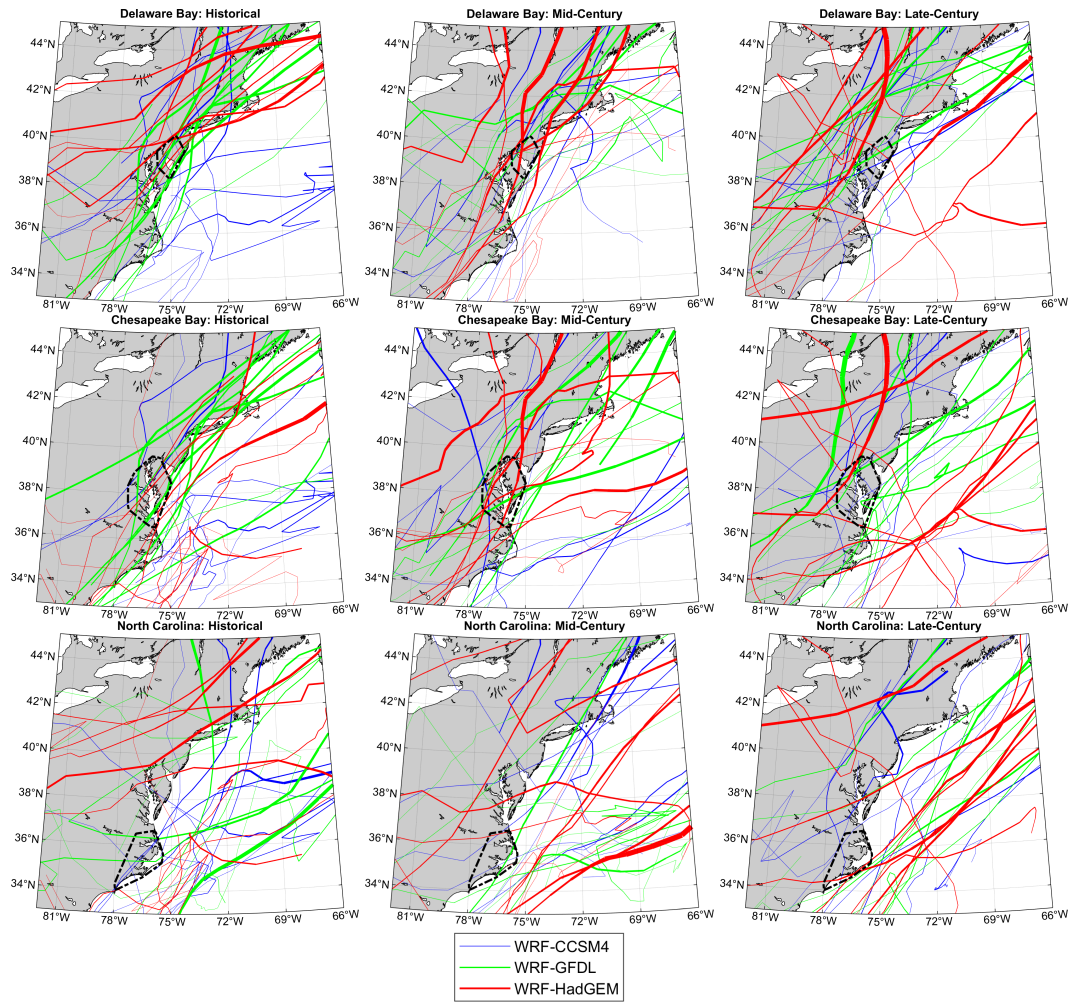


**Figure 8.** Same as Fig. 7 but for the southern subregions (top: Delaware Bay, middle: Chesapeake Bay, bottom: North Carolina).

393 WRF-CCSM4 produces no particularly strong storm tide generating ETCs affect-  
 394 ing the southern subregions (Delaware Bay, Chesapeake Bay, and North Carolina) in any  
 395 decade (Fig. 8). Regarding track patterns, there are generally more WRF-CCSM4 storm  
 396 tracks passing through and just offshore of the North Carolina and the southern end of  
 397 Chesapeake Bay in the historical decade than the future ones which could explain why  
 398 future WRF-CCSM4 generated storm tides are moderately decreased (both the 3-season  
 399 and 1-season PST) in these regions. WRF-GFDL produces a number of moderately in-  
 400 tense storms directly impacting Delaware Bay and Chesapeake Bay in the historical decade.  
 401 In future decades, WRF-GFDL storms are mostly less intense and there are fewer tracks  
 402 that directly pass through or very close to the Delaware Bay and Chesapeake Bay sub-  
 403 regions. However, WRF-GFDL storms tides are projected to be largely unchanged in  
 404 these southern subregions with some small areas in Chesapeake Bay and North Carolina  
 405 showing moderate increases. Noticeably, WRF-GFDL track angles in the historical decade  
 406 are running very close to and parallel to the coastline while there is somewhat more vari-  
 407 ation in track angles for the future decades, which could be leading to certain tributaries  
 408 of Chesapeake Bay having increased storm tides due to storm angles more favorable to  
 409 surge. Furthermore, one may note the two moderately intense ETC tracks passing through  
 410 the North Carolina subregion in the historical decade are in the west-to-east direction  
 411 which would not be as favorable to surge in Albemarle and Pamlico Sounds as those tracks  
 412 running just offshore of the subregion in the southwest-to-northeast direction plotted in  
 413 the future decades. Compared to the historical decade, WRF-HadGEM storms affect-  
 414 ing the Delaware Bay and Chesapeake Bay subregions are generally stronger and the track  
 415 angle appears to be less oblique (more south-to-north running than parallel to the coast)  
 416 in future decades. WRF-HadGEM generating storm tides in the northern areas Chesape-  
 417 peake Bay and Delaware Bay/River are indeed projected to increase in future decades  
 418 while those in the areas exposed to the open ocean decrease. There also appear to be  
 419 more intense WRF-HadGEM storms tracking just offshore, as well as a couple just in-  
 420 land, of the North Carolina subregion in the future decades. Indeed, WRF-HadGEM gen-  
 421 erated storm tides are mostly larger in the North Carolina subregion in future decades.

## 422 4 Discussion

### 423 4.1 Summary of Findings and Implications

424 Projected future changes in 1- and 3-season peak storm tide elevations along the  
 425 NEC under the RCP8.5 climate change scenario were found to range between  $\pm 0.3$  m  
 426 and  $\pm 0.5$  m, respectively. Variation due to RCM forcing is significant and generally greater  
 427 than the variation between mid-century and late-century decades for the same RCM. In  
 428 the New England and Long Island Sound subregions there is no general consensus on  
 429 mid-century or late-century changes to PST. This is similar to the findings of Lin et al.  
 430 (2019) who project a small increase to cool-season surge heights under CCSM4 GCM  
 431 forcing and a decrease under GFDL GCM forcing at Boston, MA (located in the New  
 432 England subregion) for the mid-to-late 21<sup>st</sup> century (2054-2079). In particular, at Sus-  
 433 sex County (#2) where Boston is located, our findings show little change to 1- and 3-  
 434 season PSTs under WRF-CCSM4 forcing and a larger decrease under WRF-GFDL forc-  
 435 ing. Furthermore, our findings are largely in agreement to Roberts et al. (2017); Lin et  
 436 al. (2019) at New York County (#21) where we demonstrate little change to 1- and 3-  
 437 season PST under WRF-HadGEM and WRF-CCSM4 forcing and a decrease under WRF-  
 438 GFDL forcing. Roberts et al. (2017) focused on New York City and found no significant  
 439 change to the cool-season maximum surge elevation, while Lin et al. (2019) show that  
 440 1-3 season return period surge heights at New York City were slightly increased under  
 441 CCSM4 GCM forcing and decreased under GFDL GCM forcing.

442 While there is not perfect consensus on projected changes to PST in the New York/New  
 443 Jersey Bight, Delaware Bay and Chesapeake Bay subregions, there is an indication that  
 444 storm tides will increase at counties along the Hudson River, Delaware River and north-

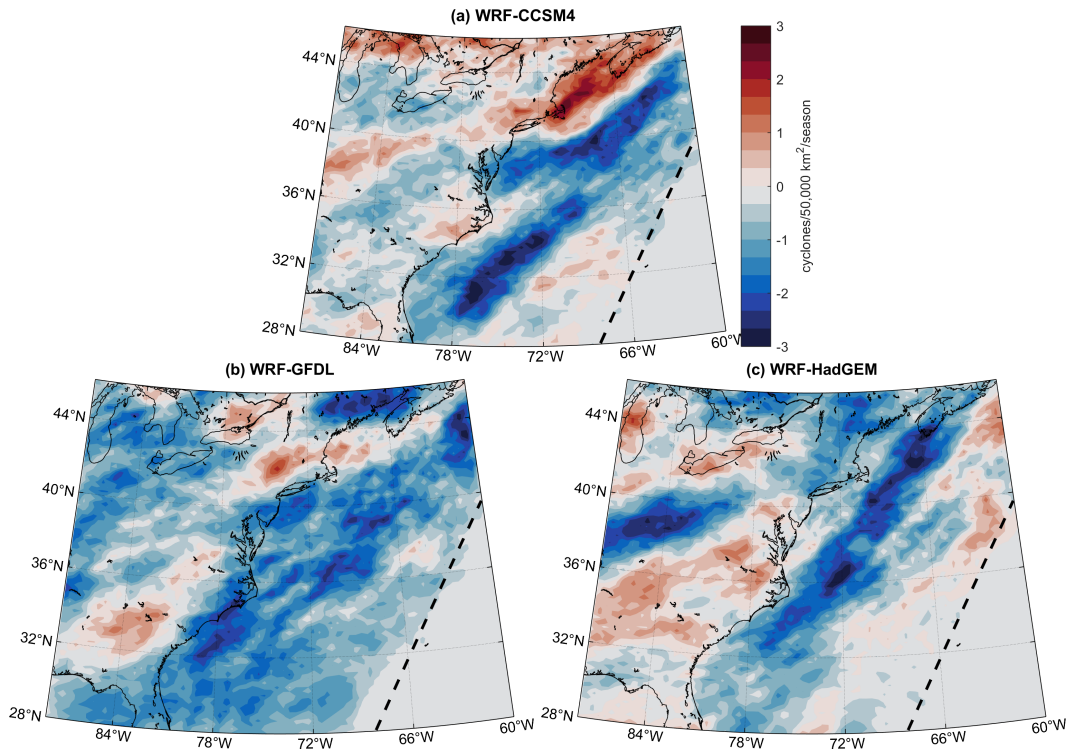


**Figure 9.** Cool-season cyclone density (number of cyclones per 50,000 km<sup>2</sup> per season) in the western North Atlantic Ocean during the late-century decade (2085-2094) as compared to the historical decade (1995-2004) for the regional climate model (RCM) simulations; (a) WRF-CCSM4, (b) WRF-GFDL, (c) WRF-HadGEM. Black dashed line indicates the edge of the RCM computational domains, explaining the null values here further offshore.

445 ern end of Chesapeake Bay, and decrease at counties facing the open ocean along the Mid-  
 446 Atlantic Bight. This pattern is clearer for the late-century decade than the mid-century,  
 447 and the magnitude of these changes varies fairly significantly between the RCMs. These  
 448 findings are essentially the opposite to projected 10-yr surge height changes under CCSM4  
 449 and GFDL GCM forcing presented in Lin et al. (2019), where decreases were predicted  
 450 in northern Chesapeake Bay and Delaware Bay and increases were predicted along the  
 451 Mid-Atlantic Bight coast. However, in this study the strongest contrasting pattern of  
 452 PST changes to the findings of Lin et al. (2019) were found under the WRF-HadGEM  
 453 forcing (Lin et al. (2019) did not show results under HadGEM GCM forcing). We found  
 454 that increased PST in the upper reaches of the large estuaries and rivers could be at-  
 455 tributed to more intense ETCs that track just inland (to the northeast) of these subre-  
 456 gions in a south-to-north direction, where southerly winds to the southeast of these ETC  
 457 centers will be favorable to generating surge in these locations. However, in the histor-  
 458 ical period there appeared to be more ETCs tracking parallel to and just offshore of the  
 459 coastline than in the future decades, likely resulting in the decreases to the PST for open  
 460 coastal facing counties. To further that point, Fig. 9 illustrates a unanimous reduction  
 461 in ETC density over most of the ocean offshore of the NEC in the late-century decade,  
 462 a general finding that is also consistent with Colle et al. (2013); Zhang and Colle (2018).

463 There is little overall consensus on PST changes in the North Carolina subregion  
 464 except for counties in the northern Albemarle Sound where the PST is projected to in-  
 465 crease by all RCMs in both future decades. In these southern counties of the NEC re-  
 466 gion the tide-surge timing is not important, particularly in the Albemarle and Pamlico

467 Sounds in which the tidal amplitude is smaller than 10 cm. Instead, storm tides are driven  
 468 by passing ETCs locally generating surge in the sounds. In contrast, the larger tidal range  
 469 in the New England, Long Island Sound, New York/New Jersey Bight and Delaware Bay  
 470 subregions leads to significant random uncertainty simply due to the phasing of the tides  
 471 and weather conditions driving surge. In fact, the direction (increase or decrease) of pro-  
 472 jected changes to 1- and 3-season PST for each RCM forcing often depends on this ran-  
 473 dom tide-surge timing in these subregions. Alternatively, the magnitude of change could  
 474 be much greater than the tidal phase-based average especially for the 3-season PST.

475 The importance of the aforementioned projected changes to the PST depend on  
 476 the relative comparisons to the magnitude and uncertainty of future SLR. Assuming that  
 477 the GCMs provide a reasonable uncertainty range of future SLR under the RCP8.5 sce-  
 478 nario (see Sect. 4.2), projected SLR is 0.2-0.8 m by mid-century and 0.4-1.3 m by late-  
 479 century. This implies that projected SLR and PST changes are about equally as impor-  
 480 tant to consider under the low-end of SLR projections for mid-century. By late-century,  
 481 low-end SLR will be slightly more important to consider for coastal flooding potential  
 482 than any storm climatology-driven PST changes. Under the high-end SLR projection,  
 483 even by mid-century potential PST changes are 2-4 times smaller in magnitude, and by  
 484 late-century PST changes are 3-6 times smaller in magnitude. Although this study, as  
 485 well as others (Roberts et al., 2017; Lin et al., 2019), suggest that SLR will likely play  
 486 a larger role in future changes to the cool-season coastal flooding potential in the 21<sup>st</sup>  
 487 century, we should consider the combination of SLR and PSTs taking into account the  
 488 full range of possibilities based on random tide-surge timing.

## 489 4.2 Uncertainties and Limitations

490 The WRF-based dynamically downscaled RCM simulations were conducted over  
 491 fairly short time periods (decadal) and a relatively small number of GCM members (three)  
 492 were used. For this reason we avoided extrapolating our results to predict 100-year or  
 493 other longer return periods using extreme value distributions. Furthermore, the RCM  
 494 simulations were originally designed to investigate the North American continental cli-  
 495 mate and not particularly focused on resolving marine climatology. Thus, the atmospheric  
 496 solution could potentially be partially influenced by the open boundary in the western  
 497 North Atlantic Ocean. However, the RCM results were carefully bias-corrected and tested  
 498 for boundary nudging effects. Future RCM simulations with greater computational re-  
 499 sources will include larger portions of the ocean, more GCM members, and longer time  
 500 periods.

501 On the hydrodynamic modeling side, the effects of wind-wave setup on coastal wa-  
 502 ter elevations have been omitted in this study, primarily because wave modeling is sig-  
 503 nificantly more computationally expensive than the hydrodynamic model. However, setup  
 504 has been found to have a relatively small contribution to peak coastal water elevations  
 505 in the NEC region (Marsooli & Lin, 2018), and is thus unlikely to impact our main find-  
 506 ing. In addition, coastal flooding has been ignored, which if considered, generally results  
 507 in lower water elevations on the ocean side compared to situations where inundation does  
 508 not (or cannot) occur (Idier et al., 2019). Nevertheless, peak storm tide elevations recorded  
 509 at the coast in our model simulations should generally be indicative of the coastal flood-  
 510 ing potential.

511 We compared the magnitude of PST changes to SLR projections which we estimated  
 512 from the parent GCMs for workflow self-consistency (avoiding external methodologies  
 513 and models). It has been shown that CMIP5 GCMs may underestimate the externally  
 514 driven anthropogenic component of SLR, particularly in the North Atlantic (Becker et  
 515 al., 2016). Compared to probabilistic SLR scenarios computed for the 21<sup>st</sup> century in  
 516 the NEC region (Sweet et al., 2017), CCSM4/GFDL estimated SLR would indeed ap-  
 517 pear to correspond closest to the “low” scenario despite representing the RCP8.5 high-

concentration pathway. However, HadGEM estimated SLR roughly corresponds to the “intermediate-high” scenario. We also note that storm tide dynamics and river discharge in the upper reaches of the estuaries and rivers may locally modulate SLR in a way that our analysis does not account for (Idier et al., 2019).

### Data Availability

Datasets for this research are available without restriction at Pringle (2020) under the Creative Commons Attribution 4.0 International license. CCSM4 climate data was downloaded from <https://www.earthsystemgrid.org/>. GFDL-ESM2G and HadGEM2-ES climate data was downloaded from <https://esgf-node.llnl.gov/search/cmip5>. Specially, we chose the ‘historical’ experiment for the historical decade and the ‘RCP8.5’ experiment for the future decades, and the ‘r1i1p1’ ensemble for both experiments. Geospatial data describing the boundaries of United States counties used in our analysis was downloaded from <https://www.census.gov/geographies/mapping-files/time-series/geo/cartographic-boundary.html>.

### Acknowledgments

WJP was supported by Laboratory Directed Research and Development (LDRD) Seed funding from Argonne National Laboratory, provided by the Director, Office of Science, of the U.S. Department of Energy under Contract No. DE-AC02-06CH11357. JW, KJR and VRK also acknowledge support from AT&T Services Inc. under a Strategic Partnership Project agreement A18131 to Argonne National Laboratory through U.S. Department of Energy contract DE-AC02-06CH11357. We acknowledge the National Energy Research Scientific Computing Center (NERSC), Argonne’s Laboratory Computing Resource Center (LCRC), and the Argonne Leadership Computing Facility (ALCF) for providing the computational resources used to conduct the WRF modeling. Similarly, we thank LCRC for providing the computational resources used to conduct the ADCIRC modeling in this study. We are grateful to Dr. Emmanouil Flaounas for providing a modified form of the CycloTrack V2 code that we used to track cyclone central SLP.

### References

- Beardsley, R. C., Chen, C., & Xu, Q. (2013). Coastal flooding in Scituate (MA): A FVCOM study of the 27 December 2010 nor’easter. *Journal of Geophysical Research: Oceans*, *118*(11), 6030–6045. doi: 10.1002/2013JC008862
- Becker, M., Karpytchev, M., Marcos, M., Jevrejeva, S., & Lennartz-Sassinek, S. (2016). Do climate models reproduce complexity of observed sea level changes? *Geophysical Research Letters*, *43*(10), 5176–5184. doi: 10.1002/2016GL068971
- Booth, J. F., Naud, C. M., & Willison, J. (2018). Evaluation of extratropical cyclone precipitation in the North Atlantic basin: An analysis of ERA-Interim, WRF, and two CMIP5 models. *Journal of Climate*, *31*(6), 2345–2360. doi: 10.1175/JCLI-D-17-0308.1
- Booth, J. F., Rieder, H. E., & Kushnir, Y. (2016). Comparing hurricane and extratropical storm surge for the Mid-Atlantic and Northeast Coast of the United States for 1979-2013. *Environmental Research Letters*, *11*(9). doi: 10.1088/1748-9326/11/9/094004
- Bunya, S., Dietrich, J. C., Westerink, J. J., Ebersole, B. A., Smith, J. M., Atkinson, J. H., . . . Roberts, H. J. (2010, feb). A High-Resolution Coupled Riverine Flow, Tide, Wind, Wind Wave, and Storm Surge Model for Southern Louisiana and Mississippi. Part I: Model Development and Validation. *Monthly Weather Review*, *138*(2), 345–377. Retrieved from <http://journals.ametsoc.org/doi/abs/10.1175/2009MWR2906.1> doi: 10.1175/2009MWR2906.1
- Catalano, A. J., & Broccoli, A. J. (2018). Synoptic characteristics of surge-

- 569 producing extratropical cyclones along the northeast coast of the United  
 570 States. *Journal of Applied Meteorology and Climatology*, 57(1), 171–184.  
 571 doi: 10.1175/JAMC-D-17-0123.1
- 572 Chang, E. K. (2013). CMIP5 projection of significant reduction in extratropical cy-  
 573 clone activity over North America. *Journal of Climate*, 26(24), 9903–9922. doi:  
 574 10.1175/JCLI-D-13-00209.1
- 575 Colle, B. A., Buonauto, F., Bowman, M. J., Wilson, R. E., Flood, R., Hunter, R.,  
 576 ... Hill, D. (2008). New York City's Vulnerability to Coastal Flooding: Storm  
 577 Surge Modeling of Past Cyclones. *Bulletin of the American Meteorological*  
 578 *Society*, 89, 829–841. doi: 10.1175/2007BAMS2401.1
- 579 Colle, B. A., Rojowsky, K., & Buonaito, F. (2010). New York city storm  
 580 surges: Climatology and an analysis of the wind and cyclone evolution.  
 581 *Journal of Applied Meteorology and Climatology*, 49(1), 85–100. doi:  
 582 10.1175/2009JAMC2189.1
- 583 Colle, B. A., Zhang, Z., Lombardo, K. A., Chang, E., Liu, P., & Zhang, M.  
 584 (2013). Historical evaluation and future prediction of eastern North Amer-  
 585 ican and Western Atlantic extratropical cyclones in the CMIP5 models  
 586 during the cool season. *Journal of Climate*, 26(18), 6882–6903. doi:  
 587 10.1175/JCLI-D-12-00498.1
- 588 Egbert, G. D., & Erofeeva, S. Y. (2019). *TPXO9-Atlas*. Retrieved from [http://](http://volkov.oce.orst.edu/tides/tpxo9\_atlas.html)  
 589 [volkov.oce.orst.edu/tides/tpxo9\\\_atlas.html](http://volkov.oce.orst.edu/tides/tpxo9\_atlas.html)
- 590 European Centre for Medium-Range Weather Forecasts. (2019). *ERA5 Reanalysis*  
 591 *(0.25 Degree Latitude-Longitude Grid)*. Boulder, CO: Research Data Archive  
 592 at the National Center for Atmospheric Research, Computational and Infor-  
 593 mation Systems Laboratory. Retrieved from [https://doi.org/10.5065/](https://doi.org/10.5065/BH6N-5N20)  
 594 [BH6N-5N20](https://doi.org/10.5065/BH6N-5N20) doi: 10.5065/BH6N-5N20
- 595 Flaounas, E., Kotroni, V., Lagouvardos, K., & Flaounas, I. (2014). CycloTRACK  
 596 (v1.0)-tracking winter extratropical cyclones based on relative vorticity: Sen-  
 597 sitivity to data filtering and other relevant parameters. *Geoscientific Model*  
 598 *Development*, 7(4), 1841–1853. doi: 10.5194/gmd-7-1841-2014
- 599 Hope, M. E., Westerink, J. J., Kennedy, A. B., Kerr, P. C., Dietrich, J. C., Dawson,  
 600 C., ... Westerink, L. G. (2013, sep). Hindcast and validation of Hurricane Ike  
 601 (2008) waves, forerunner, and storm surge. *Journal of Geophysical Research:*  
 602 *Oceans*, 118(9), 4424–4460. Retrieved from [http://doi.wiley.com/10.1002/](http://doi.wiley.com/10.1002/jgrc.20314)  
 603 [jgrc.20314](http://doi.wiley.com/10.1002/jgrc.20314) doi: 10.1002/jgrc.20314
- 604 Horsburgh, K. J., & Wilson, C. (2007). Tide-surge interaction and its role in the dis-  
 605 tribution of surge residuals in the North Sea. *Journal of Geophysical Research:*  
 606 *Oceans*, 112(8), 1–13. doi: 10.1029/2006JC004033
- 607 Idier, D., Bertin, X., Thompson, P., & Pickering, M. D. (2019). Interactions Between  
 608 Mean Sea Level, Tide, Surge, Waves and Flooding: Mechanisms and Contri-  
 609 butions to Sea Level Variations at the Coast. *Surveys in Geophysics*, 40(6),  
 610 1603–1630. Retrieved from <https://doi.org/10.1007/s10712-019-09549-5>  
 611 doi: 10.1007/s10712-019-09549-5
- 612 Lin, N., Marsooli, R., & Colle, B. A. (2019). Storm surge return levels in-  
 613 duced by mid-to-late-twenty-first-century extratropical cyclones in the  
 614 Northeastern United States. *Climatic Change*, 154(1-2), 143–158. doi:  
 615 10.1007/s10584-019-02431-8
- 616 Long, Z., Perrie, W., Gyakum, J., Laprise, R., & Caya, D. (2009). Scenario changes  
 617 in the climatology of winter midlatitude cyclone activity over eastern North  
 618 America and the Northwest Atlantic. *Journal of Geophysical Research Atmo-*  
 619 *spheres*, 114(12), 1–13. doi: 10.1029/2008JD010869
- 620 Luettich, R. A., & Westerink, J. J. (2004). *Formulation and Numerical Implemen-*  
 621 *tation of the 2D/3D ADCIRC Finite Element Model Version 44.XX* (Tech.  
 622 Rep.). University of North Carolina at Chapel Hill & University of Notre  
 623 Dame.

- 624 Marsooli, R., & Lin, N. (2018). Numerical Modeling of Historical Storm  
 625 Tides and Waves and Their Interactions Along the U.S. East and Gulf  
 626 Coasts. *Journal of Geophysical Research: Oceans*, *123*(5), 3844–3874. doi:  
 627 10.1029/2017JC013434
- 628 Marsooli, R., Lin, N., Emanuel, K., & Feng, K. (2019). Climate change exacerbates  
 629 hurricane flood hazards along U.S. Atlantic coast in spatially varying patterns.  
 630 *Nature Communications*, *10*, 3785. Retrieved from [http://dx.doi.org/  
 631 10.1038/s41467-019-11755-z](http://dx.doi.org/10.1038/s41467-019-11755-z) doi: 10.1038/s41467-019-11755-z
- 632 Parker, B. B. (2007). *Tidal analysis and prediction*. Silver Spring, MD.
- 633 Pringle, W. J. (2020). *Projected Changes to Cool-Season Storm Tides along the  
 634 Northeastern U.S. Coast: Dataset*. Zenodo. doi: 10.5281/zenodo.4320052
- 635 Pringle, W. J., & Roberts, K. J. (2020). *CHLNDDEV/OceanMesh2D: OceanMesh2D  
 636 V3.0.0*. Zenodo. doi: 10.5281/zenodo.3721137
- 637 Pringle, W. J., Wirasaet, D., Roberts, K. J., & Westerink, J. (2020). Global  
 638 Storm Tide Modeling with ADCIRC v55: Unstructured Mesh Design and  
 639 Performance. *Geoscientific Model Development Discussions*, in review. doi:  
 640 10.5194/gmd-2020-123
- 641 Riahi, K., Rao, S., Krey, V., Cho, C., Chirkov, V., Fischer, G., ... Rafaj, P. (2011).  
 642 RCP 8.5-A scenario of comparatively high greenhouse gas emissions. *Climatic  
 643 Change*, *109*(1), 33–57. doi: 10.1007/s10584-011-0149-y
- 644 Roberts, K. J. (2015). *An Application of Regression for Storm Surge Prediction  
 645 along the New York/New Jersey Coast in Climate Models* (Masters Thesis,  
 646 Stony Brook University). Retrieved from [http://hdl.handle.net/11401/  
 647 76207](http://hdl.handle.net/11401/76207)
- 648 Roberts, K. J., Colle, B. A., & Korfe, N. (2017). Impact of simulated twenty-first-  
 649 century changes in extratropical cyclones on coastal flooding at the Battery,  
 650 New York City. *Journal of Applied Meteorology and Climatology*, *56*(2), 415–  
 651 432. doi: 10.1175/JAMC-D-16-0088.1
- 652 Roberts, K. J., Pringle, W. J., & Westerink, J. J. (2019). OceanMesh2D 1.0:  
 653 MATLAB-based software for two-dimensional unstructured mesh generation in  
 654 coastal ocean modeling. *Geoscientific Model Development*, *12*, 1847–1868. doi:  
 655 10.5194/gmd-12-1847-2019
- 656 Roberts, K. J., Pringle, W. J., Westerink, J. J., Contreras, M. T., & Wirasaet, D.  
 657 (2019). On the automatic and a priori design of unstructured mesh resolution  
 658 for coastal ocean circulation models. *Ocean Modelling*, *144*, 101509. doi:  
 659 10.1016/j.ocemod.2019.101509
- 660 Schwalm, C. R., Glendon, S., & Duffy, P. B. (2020). RCP8.5 tracks cumulative CO2  
 661 emissions. *Proceedings of the National Academy of Sciences*, *117*(33), 19656–  
 662 19657. doi: 10.1073/pnas.2007117117
- 663 Seiler, C., Zwiers, F. W., Hodges, K. I., & Scinocca, J. F. (2018). How does dy-  
 664 namical downscaling affect model biases and future projections of explosive  
 665 extratropical cyclones along North America’s Atlantic coast? *Climate Dynam-  
 666 ics*, *50*(1-2), 677–692. doi: 10.1007/s00382-017-3634-9
- 667 Sherwood, S. C., Bony, S., & Dufresne, J. L. (2014). Spread in model climate sensi-  
 668 tivity traced to atmospheric convective mixing. *Nature*, *505*(7481), 37–42. doi:  
 669 10.1038/nature12829
- 670 Sweet, W. V., Kopp, R. E., Weaver, C. P., Obeysekera, J., Horton, R. M., Thieler,  
 671 E. R., & Zervas, C. (2017). *Global and Regional Sea Level Rise Scenar-  
 672 ios for the United States* (Tech. Rep. No. NOS CO-OPS 083). NOAA/NOS  
 673 Center for Operational Oceanographic Products and Services. Retrieved  
 674 from [https://tidesandcurrents.noaa.gov/publications/techrpt83{\\\_  
 675 \\_}Global{\\\_}and{\\\_}Regional{\\\_}SLR{\\\_}Scenarios{\\\_}for{\\\_}the{\\\_  
 676 \\_}US{\\\_}final.pdf](https://tidesandcurrents.noaa.gov/publications/techrpt83/\_Global{\_}and{\_}Regional{\_}SLR{\_}Scenarios{\_}for{\_}the{\_}US{\_}final.pdf)
- 677 Taylor, K. E., Stouffer, R. J., & Meehl, G. A. (2012). An overview of CMIP5 and  
 678 the experiment design. *Bulletin of the American Meteorological Society*, *93*(4),

- 679 485–498. doi: 10.1175/BAMS-D-11-00094.1
- 680 Teng, H., Washington, W. M., & Meehl, G. A. (2008). Interannual varia-  
681 tions and future change of wintertime extratropical cyclone activity over  
682 North America in CCSM3. *Climate Dynamics*, 30(7-8), 673–686. doi:  
683 10.1007/s00382-007-0314-1
- 684 Tozer, B., Sandwell, D. T., Smith, W. H., Olson, C., Beale, J. R., & Wessel, P.  
685 (2019). Global Bathymetry and Topography at 15 Arc Sec: SRTM15+. *Earth  
686 and Space Science*, 6(10), 1847–1864. doi: 10.1029/2019EA000658
- 687 Wang, J., & Kotamarthi, V. R. (2015). High-resolution dynamically downscaled pro-  
688 jections of precipitation in the mid and late 21st century over North America.  
689 *Earth's Future*, 3(7), 268–288. doi: 10.1002/2015EF000304
- 690 Westerink, J. J., Luettich, R. A., Feyen, J. C., Atkinson, J. H., Dawson, C.,  
691 Roberts, H. J., ... Pourtaheri, H. (2008, mar). A Basin- to Channel-  
692 Scale Unstructured Grid Hurricane Storm Surge Model Applied to South-  
693 ern Louisiana. *Monthly Weather Review*, 136(3), 833–864. Retrieved from  
694 <http://journals.ametsoc.org/doi/abs/10.1175/2007MWR1946.1> doi:  
695 10.1175/2007MWR1946.1
- 696 Zhang, Z., & Colle, B. A. (2018). Impact of dynamically downscaling two CMIP5  
697 models on the historical and future changes in winter extratropical cyclones  
698 along the East Coast of North America. *Journal of Climate*, 31(20), 8499–  
699 8525. doi: 10.1175/JCLI-D-18-0178.1
- 700 Zobel, Z., Wang, J., Wuebbles, D. J., & Kotamarthi, V. R. (2018). Evaluations of  
701 high-resolution dynamically downscaled ensembles over the contiguous United  
702 States. *Climate Dynamics*, 50(3-4), 863–884. doi: 10.1007/s00382-017-3645-6

Figure 1.

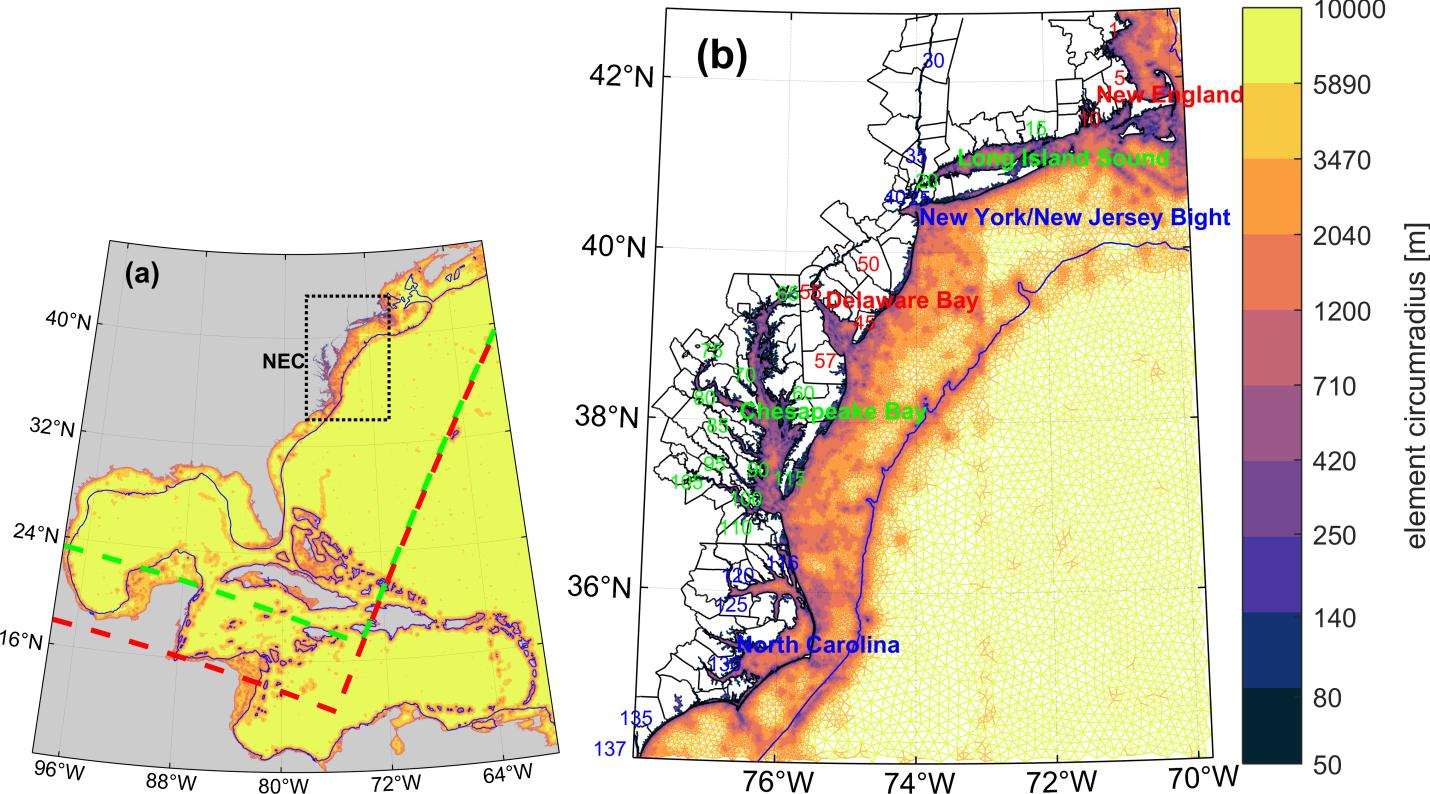
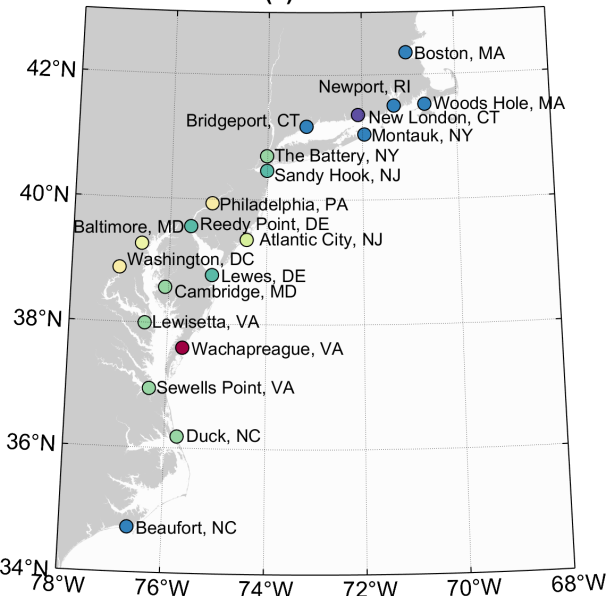
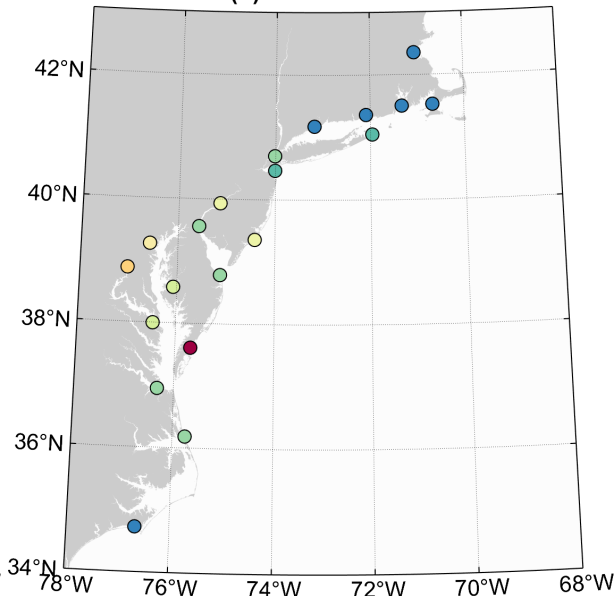


Figure 2.

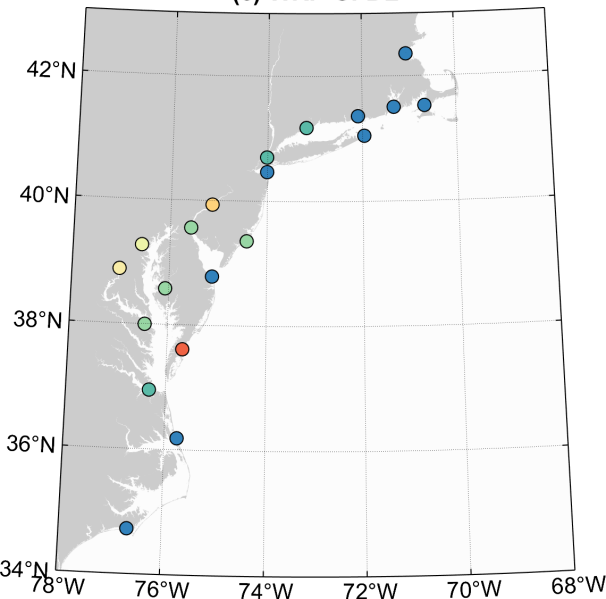
(a) ERA5



(b) WRF-CCSM4



(c) WRF-GFDL



(d) WRF-HadGEM

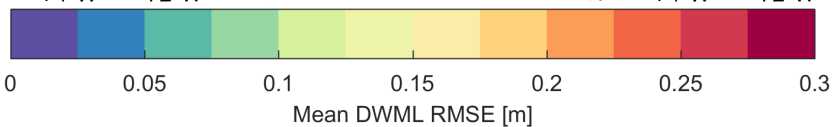
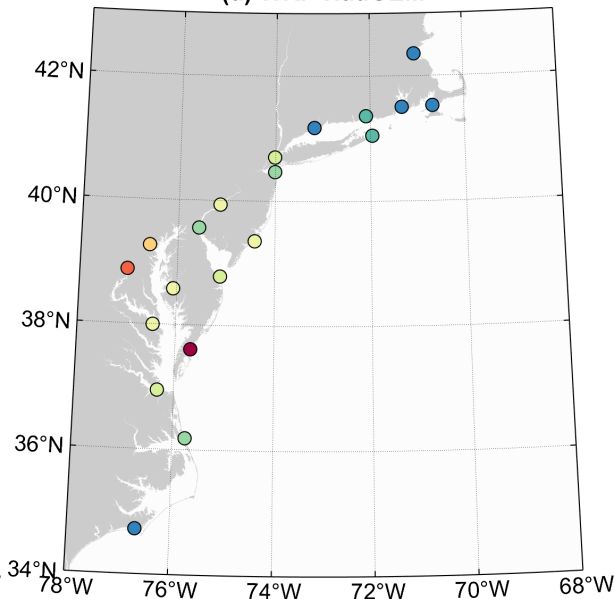
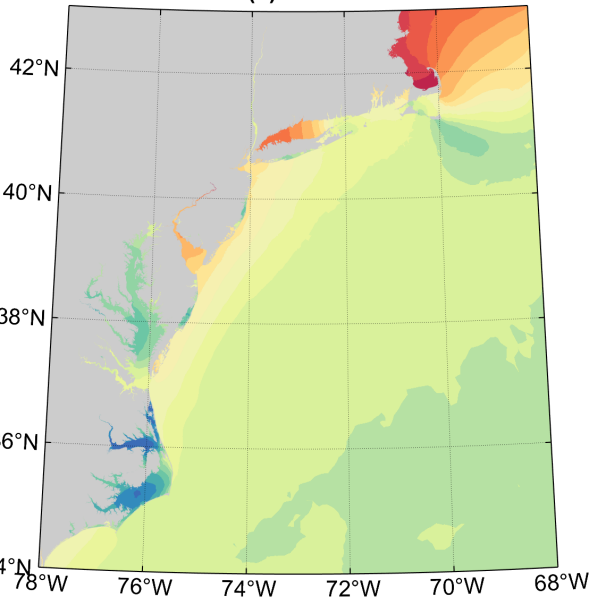
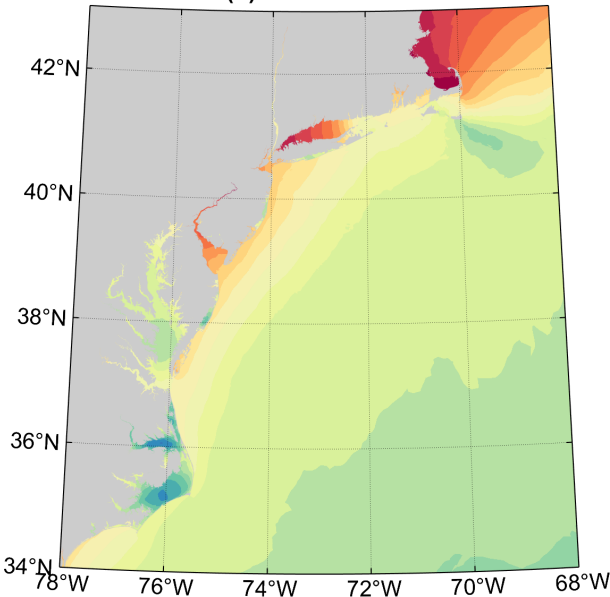
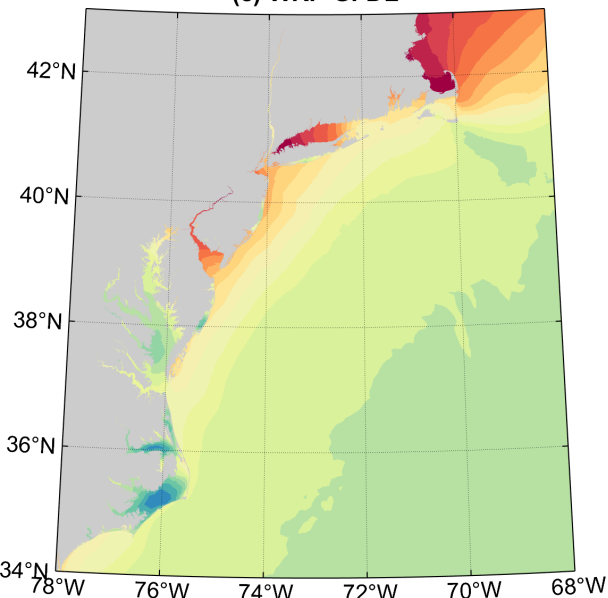
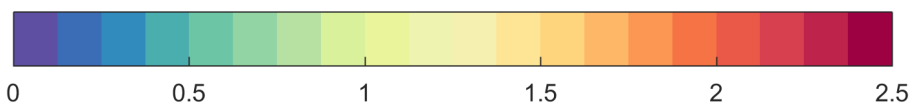
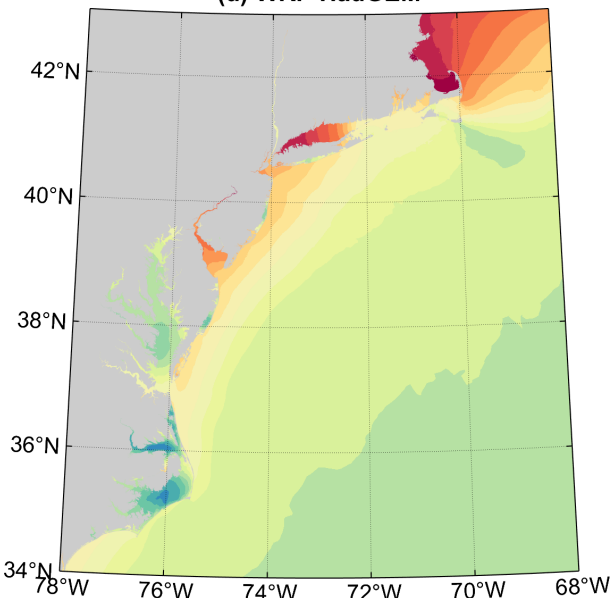


Figure 3.

**(a) ERA5****(b) WRF-CCSM4****(c) WRF-GFDL****(d) WRF-HadGEM**

3-season Peak Storm Tide Elevation [m]

**Figure 4.**

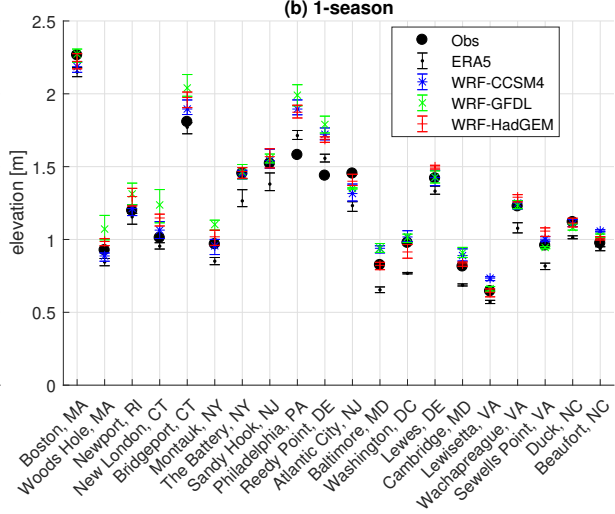
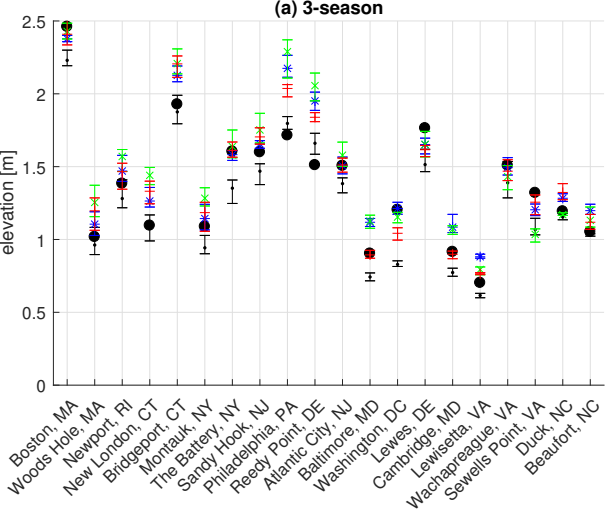


Figure 5.

## 3-season PST at Counties

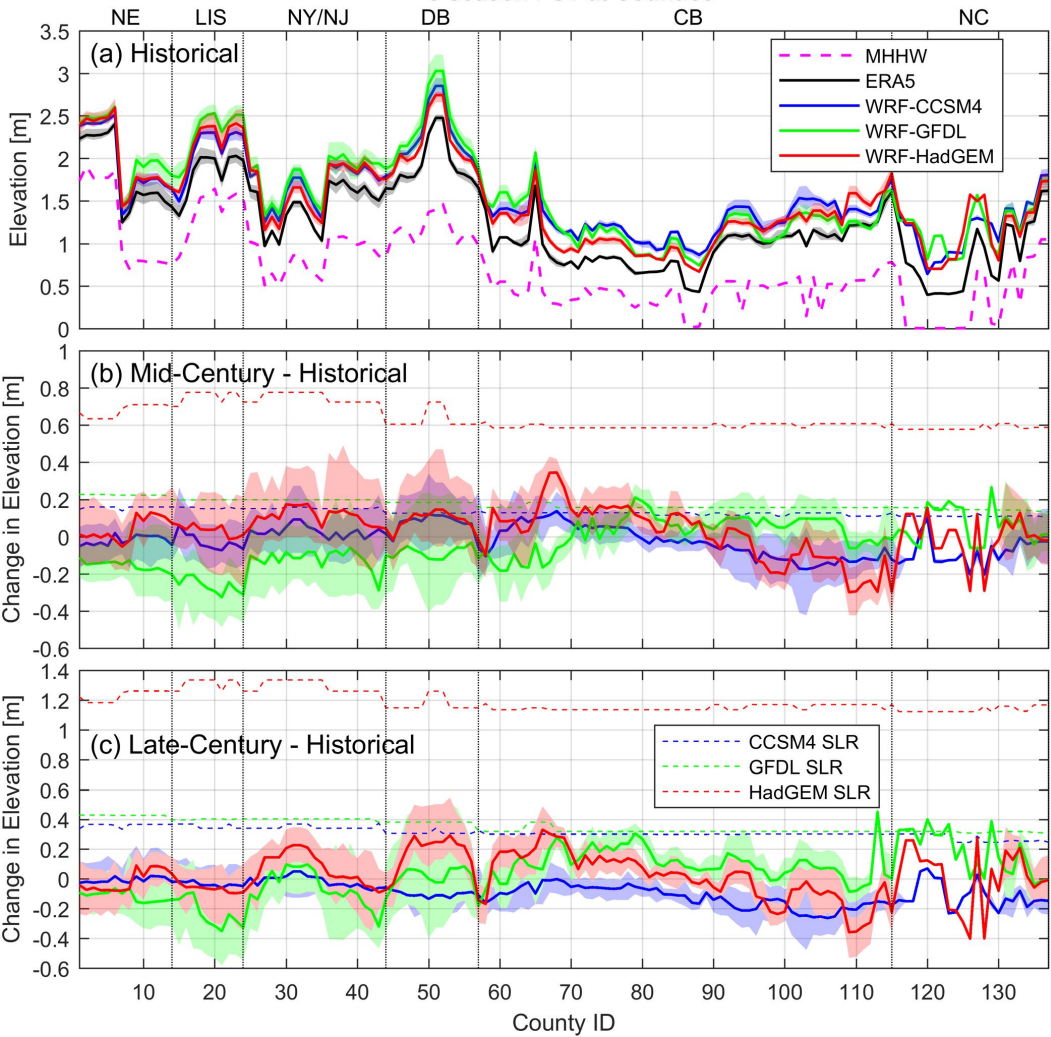
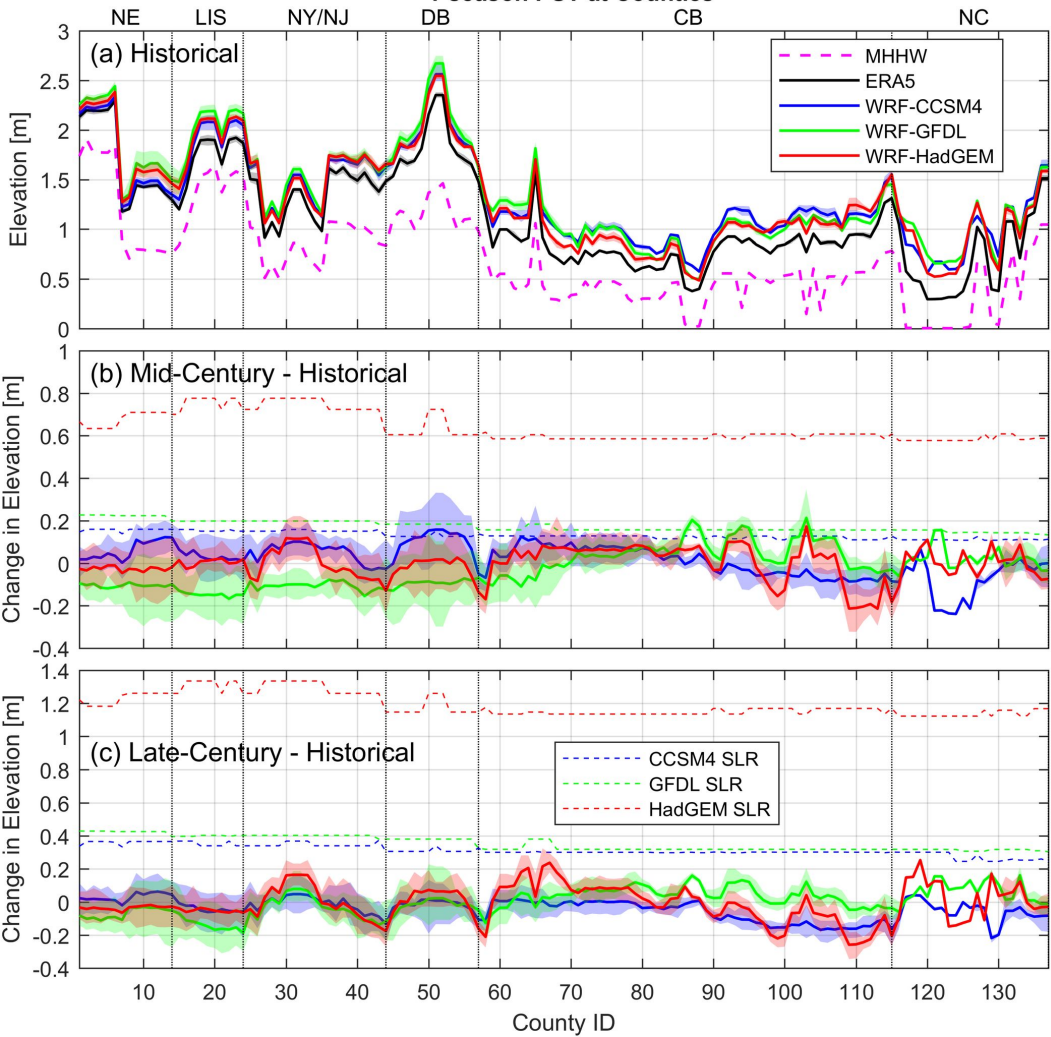


Figure 6.

## 1-season PST at Counties



**Figure 7.**

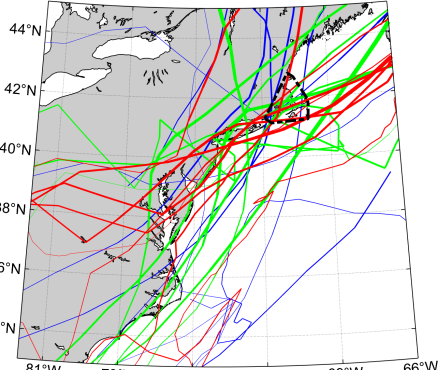
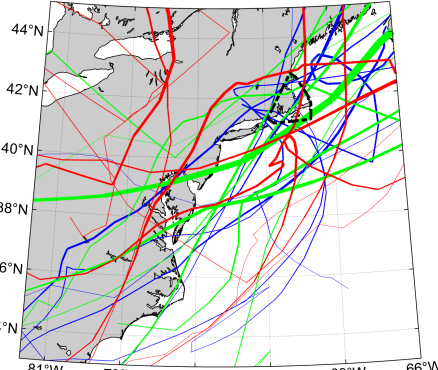
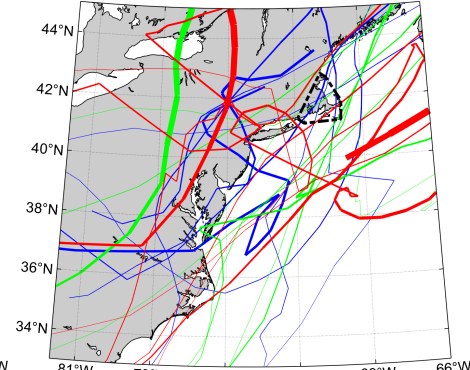
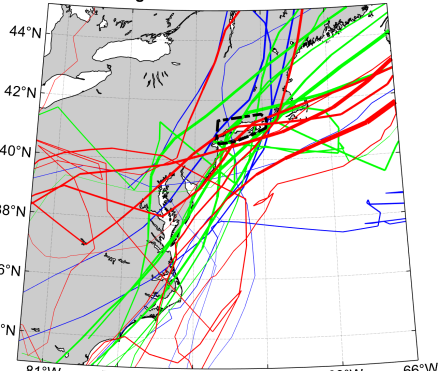
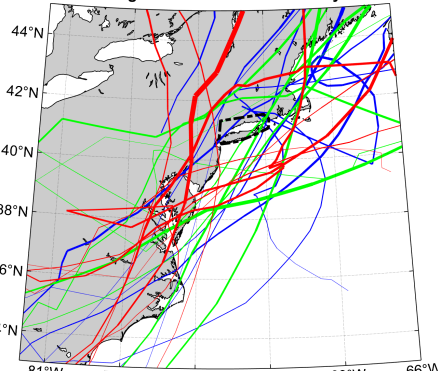
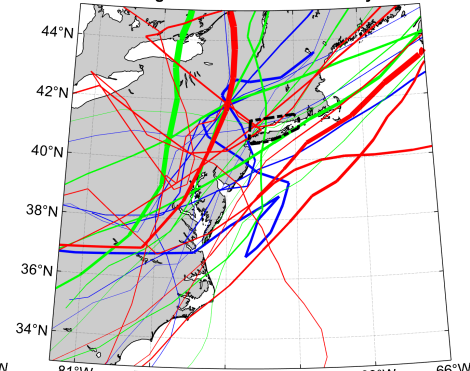
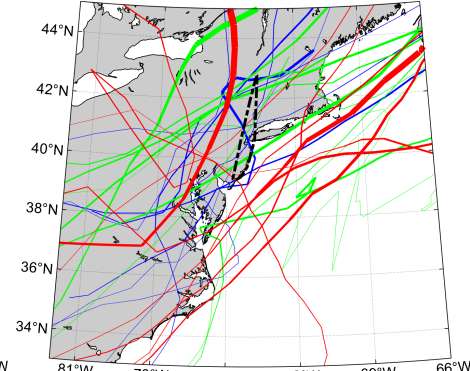
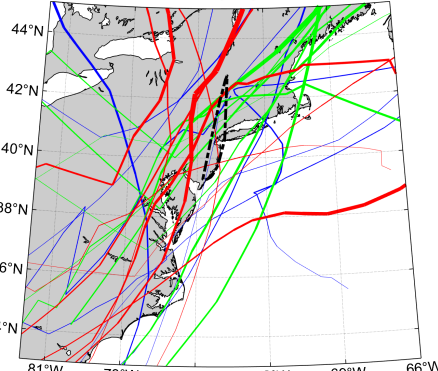
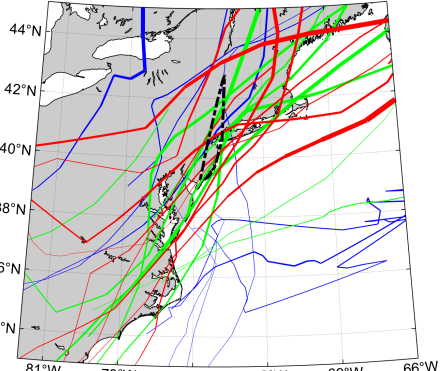
**New England: Historical****Long Island Sound: Historical****New England: Mid-Century****Long Island Sound: Mid-Century****New England: Late-Century****Long Island Sound: Late-Century****New York/New Jersey Bight: Historical****New York/New Jersey Bight: Mid-Century****New York/New Jersey Bight: Late-Century**

Figure 8.

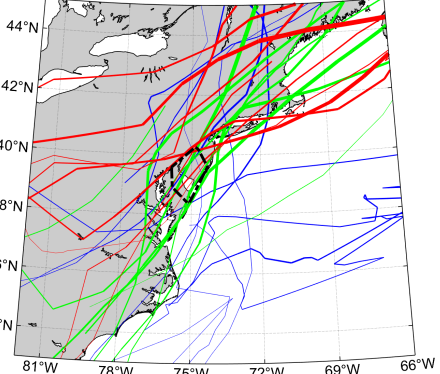
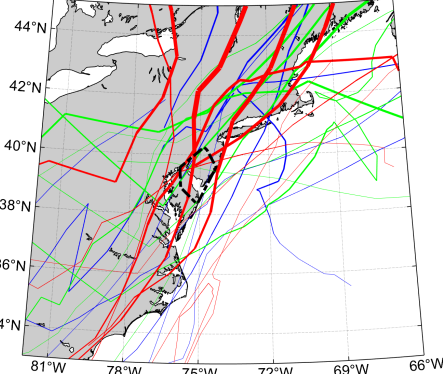
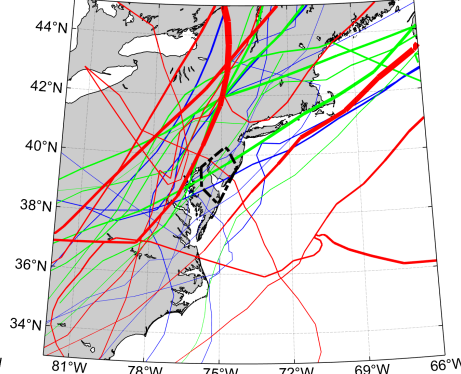
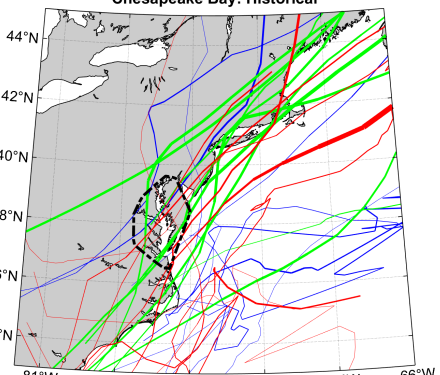
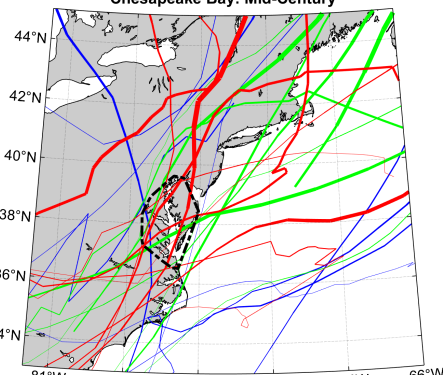
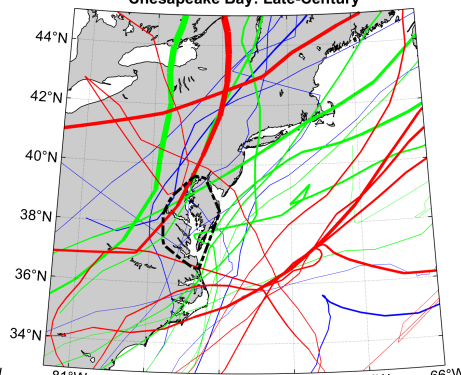
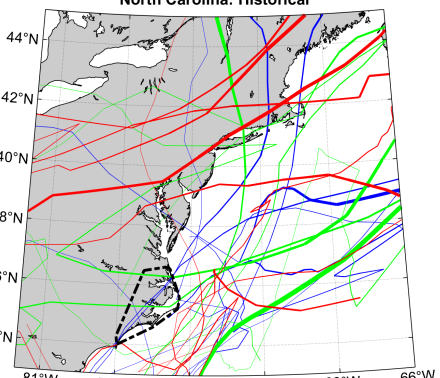
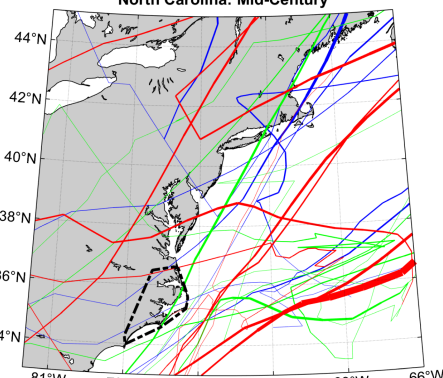
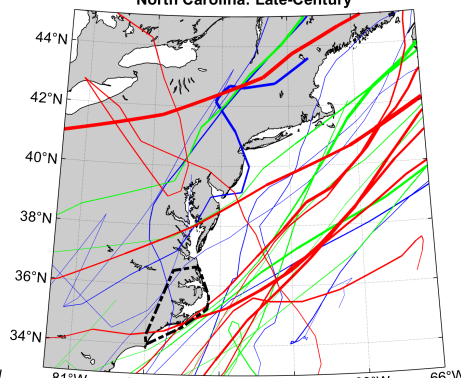
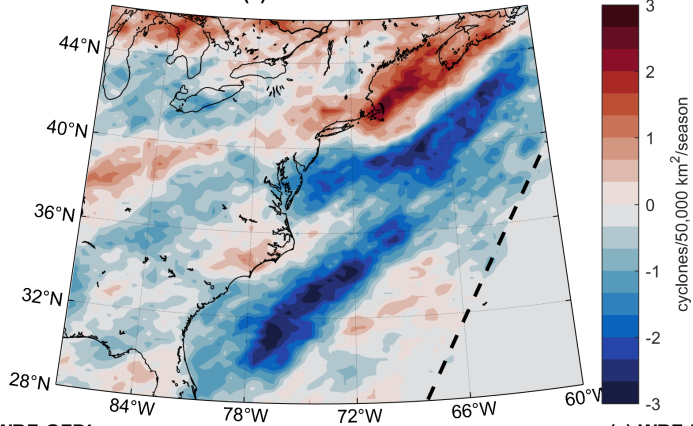
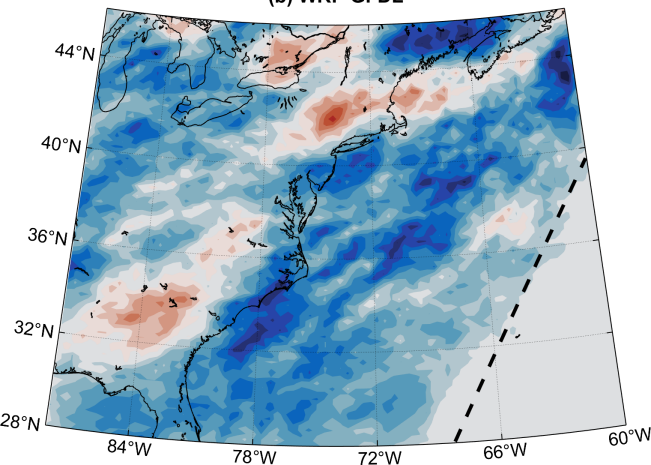
**Delaware Bay: Historical****Delaware Bay: Mid-Century****Delaware Bay: Late-Century****Chesapeake Bay: Historical****Chesapeake Bay: Mid-Century****Chesapeake Bay: Late-Century****North Carolina: Historical****North Carolina: Mid-Century****North Carolina: Late-Century**

Figure 9.

(a) WRF-CCSM4



(b) WRF-GFDL



(c) WRF-HadGEM

